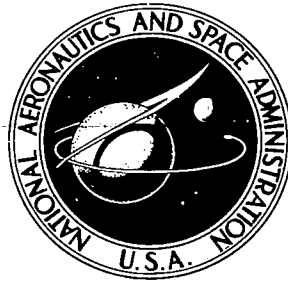


NASA CONTRACTOR
REPORT

NASA CR-2062



NASA-CR-

006 11152



TECH LIBRARY KAFB, NM

LOAN COPY: RETURN TO
AFWL (DOUL)
KIRTLAND AFB, N. M.

ATMOSPHERIC PRESSURE, DENSITY,
TEMPERATURE AND WIND VARIATIONS
BETWEEN 50 AND 200 KM

by C. G. Justus and Arthur Woodrum

Prepared by

GEORGIA INSTITUTE OF TECHNOLOGY
Atlanta, Ga. 30332

for George C. Marshall Space Flight Center

NATIONAL AERONAUTICS AND SPACE ADMINISTRATION • WASHINGTON, D. C. • MAY 1972



0061152

TECHNICAL REPORT FORM 1410-100

1. REPORT NO. NASA CR-2062	2. GOVERNMENT ACCESSION NO.	3. RECIPIENT'S CATALOG NO.	
4. TITLE AND SUBTITLE ATMOSPHERIC PRESSURE, DENSITY, TEMPERATURE AND WIND VARIATIONS BETWEEN 50 AND 200 KM		5. REPORT DATE May 1972	
7. AUTHOR(S) C. G. Justus and Arthur Woodrum		6. PERFORMING ORGANIZATION CODE E-16-612	
9. PERFORMING ORGANIZATION NAME AND ADDRESS School of Aerospace Engineering Georgia Institute of Technology Atlanta, Georgia 30332		10. WORK UNIT NO.	
12. SPONSORING AGENCY NAME AND ADDRESS NASA Washington, D. C. 20546		11. CONTRACT OR GRANT NO. NAS8-26658	
15. SUPPLEMENTARY NOTES		13. TYPE OF REPORT & PERIOD COVERED CONTRACTOR REPORT	
16. ABSTRACT Data on atmospheric pressure, density, temperature and winds between 50 and 200 km were collected from sources including Meteorological Rocket Network data, ROBIN falling sphere data, grenade release and pitot tube data, meteor winds, chemical release winds, satellite data, and others. These data were analyzed by a daily difference method and results on the distribution statistics, magnitude, and spatial structure of the irregular atmospheric variations are presented. Time structures of the irregular variations were determined by the analysis of residuals from harmonic analysis of time series data. The observed height variations of irregular winds and densities are found to be in accord with a theoretical relation between these two quantities developed by E. B. Miller for gravity waves. The latitude variations (at 50 - 60 km height) show an increasing trend with latitude. A possible explanation of the unusually large irregular wind magnitudes of the White Sands MRN data is given in terms of mountain wave generation by the Sierra Nevada range about 1000 km west of White Sands. An analytical method is developed which, based on an analogy of the irregular motion field with axisymmetric turbulence, allows measured or model correlation or structure functions to be used to evaluate the effective frequency spectra of scalar and vector quantities of a spacecraft moving at any speed and at any trajectory elevation angle.			
17. KEY WORDS	18. DISTRIBUTION STATEMENT 13		
19. SECURITY CLASSIF. (of this report) Unc1	20. SECURITY CLASSIF. (of this page) Unc1	21. NO. OF PAGES 77	22. PRICE \$3.00



TABLE OF CONTENTS

Section	Page
1. BACKGROUND	1
2. DATA ANALYSIS AND INTERPRETATIONS	8
3. PROBABILITY DISTRIBUTIONS AND MAGNITUDES	16
4. VERTICAL STRUCTURE FUNCTION DATA	40
5. HORIZONTAL STRUCTURE FUNCTION DATA	52
6. TIME STRUCTURE FUNCTION DATA	59
7. THE EFFECTIVE FREQUENCY SPECTRUM ENCOUNTERED BY A SPACECRAFT	63

ACKNOWLEDGMENTS

Our thanks go to many people who have supplied us with data and information: to Mr. Dale Johnson of NASA Huntsville who sent us the MRN data for 1964 - 1968 on magnetic tape, to Mr. Robert W. Lenhard of AFCRL who was instrumental in our obtaining magnetic tapes of the ARCAS-ROBIN data, to Dr. Arnold A. Barnes of AFCRL and Dr. A. Spizzichino who supplied Dr. R. G. Roper of Georgia Tech with the meteor wind data from Durham, New Hampshire and Garchy, France, to Dr. Roper who performed the Groves analysis of the meteor data, to Dr. John Theon of NASA Goddard who sent us the collected reports of their grenade release results, and to Mr. J. F. Bedinger of GCA and Dr. N. W. Rosenberg of AFCRL who supplied us with reports and other data on chemical release winds.

1. BACKGROUND

Serious exploration of the upper atmosphere began in the 1950's as the possibility of artificial earth satellites appeared on the horizon. In 1960, it was shown by Hines⁽¹⁾ that much of the observational data on the upper atmospheric variations could be interpreted in terms of gravity waves. Although the original theory considered only an isothermal atmosphere, with no viscosity or heat conduction it did explain several features which are consistent with observation. Among these features were the large ratio between horizontal and vertical wavelengths, the increasing amplitude with height, and the downward phase propagation associated with upward energy propagation. Later advances in the theoretical considerations analyzed the effects of realistic temperature profiles⁽²⁾, viscous damping and thermal conductivity^(3,4), wind shear⁽⁵⁾, critical layers⁽⁶⁾, and ohmic losses^(7,8).

Although there is no unambiguous resolution of gravity waves in the upper atmosphere (i.e. simultaneous observation of amplitudes, phases, and frequency sufficient to verify propagation according to the theoretical dispersion equation) there is strong circumstantial evidence for their occurrence. Table 1 summarizes some of this observational evidence. This table was adapted from Bauer et al⁽²⁶⁾. Tables 2 and 3, adapted from Bauer's report and from Tchen⁽²⁷⁾ summarize the mechanisms for the generation and the dissipation of gravity waves. In addition to the dissipation effects of Table 3, gravity waves can also be prevented from propagating to adjacent layers of the atmosphere by the effects of ducting⁽⁴¹⁾.

It should be emphasized, however, that despite the large body of observations summarized in the above tables, that in no cases have sufficient parameters

TABLE 1. EVIDENCE FOR THE OCCURRENCE OF GRAVITY
WAVES IN THE ATMOSPHERE

<u>Observation</u>	<u>Altitude Range</u>	<u>References</u>
1. Wave structure on clouds	0 - 10 km	
2. Pressure variations observed on microbarographs	low altitudes	
3. Mountain waves (well known to sailplane pilots)	0 - 10 km	
4. Wave structure on wind profiles from ROBIN balloons and smoke trails	30 - 70 km	Cole and Kantor ⁽⁹⁾ Mahoney ⁽¹⁰⁾
5. Wave structure on pitot tube and grenade temperature profiles	30 - 120 km	Theon et al. ⁽¹¹⁾
6. Wave patterns on noctilucent clouds	80 - 90 km	Witt ⁽¹²⁾ , Hines ⁽¹³⁾ Haurwitz and Fogle ⁽¹⁴⁾
7. Irregular meteor wind variations	80 - 100 km	Greenhow and Neufeld ⁽¹⁵⁾ Justus and Roper ⁽¹⁶⁾ Spizzichino and Revah ⁽¹⁷⁾
8. Chemical releases show winds with a wave structure	80 - 160 km	Kochanski ⁽¹⁸⁾
9. Wave structure in rocket probe measured temperature profiles	100 - 170 km	Knudson and Sharp ⁽¹⁹⁾
10. Occasional sinusoidal variation in ion temperature observed on satellite-borne instruments	200 - 250 km	Harris, et al. ⁽²⁰⁾
11. Thomson scatter radar observations of waves	F - region (200 - 300 km)	Vasseur and Waldteufel ⁽²¹⁾

TABLE 1. Continued

	<u>Observation</u>	<u>Altitude Range</u>	<u>References</u>
12.	Various ionospheric irregularities, such as Sudden Ionospheric Disturbances (SIDs)	200 - 300 km	Georges ^(22,23)
13.	Certain ionospheric disturbances correlate with severe local storms in the troposphere	F2 - region	Baker and Davies ⁽²⁴⁾ Georges ⁽²³⁾ Davies and Jones ⁽²⁵⁾

TABLE 2. POSSIBLE MECHANISMS FOR THE GENERATION
OF GRAVITY WAVES IN THE ATMOSPHERE

1. Generation of propagating wave by surface frontal systems (Hines⁽²⁸⁾).
2. Generation of waves induced by jet streams (Hines^(13,28)).
3. Winds blowing transversely over mountain ranges, or equivalent effects on the air motion produced by warm cities, etc., either directly or by vortices produced by air flows over non-uniform surfaces (cf. Eckart⁽²⁹⁾, p. 120).
4. Volcanic eruptions, thunderstorms, hurricanes, typhoons, tornadoes, and similar dramatic meteorological disturbances.
5. Temperature inversions in the lower portion of the atmosphere produce a fluctuating wind, which correlates with gravity waves observed on clouds at the lower levels (cf. Eckart⁽²⁹⁾, p. 121).
6. Solar heating and photodissociation with the stratosphere/mesosphere, leading to local expansion.
7. Photochemical "pumping" by either oxygen dissociation (Leovy) or ozone dissociation (Shere and Eberstein⁽³⁰⁾).
8. Auroral currents (Blumen and Hendl⁽³¹⁾, Chimonas and Hines⁽³²⁾, Testud⁽³³⁾).
9. Turbulent motion in the 55 - 60 km region of the atmosphere (Murphy et al.⁽³⁴⁾).
10. In situ generation of gravity waves from non-linear interactions of tidal modes (Justus⁽³⁵⁾).

TABLE 3. POSSIBLE MECHANISMS FOR THE DISSIPATION
OF ATMOSPHERIC GRAVITY WAVES

1. Mode coupling i.e., nonlinear processes in which the energy goes from one wave into others (Spizzichino⁽³⁵⁾).
2. Frictional damping, produced by viscosity and thermal conductivity Pitteway and Hines⁽³⁾.
3. Generation of turbulence (Hodges⁽³⁷⁾, Tchen⁽²⁷⁾).
4. Vibrational relaxation (Bauer and Podney⁽³⁹⁾ -- see also item 7 in Table 2).
5. Plasma damping effects (Liu and Yeh⁽³⁹⁾).
6. Radiation damping (Gille⁽³⁹⁾).
7. Chemical relaxation, or the shift of the O₂ = 2 O balance under the influence of the sound wave.
8. Diffusion (in the case of a gas mixture).
9. Cascade of energy up the spectrum to larger scales because of a $k^{-5/3}$ two dimensional horizontal spectrum (see Section 5 of this report, see also item 1 in this table).

been measured simultaneously to establish whether the observed wave-like structure has either the precise horizontal to vertical scale ratio for a given frequency wave length combination as required by the gravity wave dispersion relations, or the appropriate relative phase between the velocity, pressure, density, and temperature variations. Since the total variations are made up of such phenomena as planetary wave, synoptic variations, tides, gravity wave, and turbulence, it is not surprising that the gravity wave components lack accurate observational resolution, in view of the difficulties in obtaining the spatial or time resolution adequate for their detection and delineation⁽⁴²⁾.

In view of the limitations of observation data available, the best approach for establishing values of parameters is probably a statistical approach such as that applied by Woodrum, Justus, and Roper^(43,44) to chemical release and meteor wind data. This approach considers the statistical properties of the non-diurnally-repeating components of wind (or temperature, etc.) and allows estimation of amplitudes and probability distribution. Structure functions of the velocity differences also indicate possible frequency spectra, and vertical wave length spectra. Similar structure functions of velocity differences over spatial separations⁽¹⁶⁾ indicate possible horizontal wave length spectra. This type of statistical approach is desirable since isolated single gravity wave components will not always be encountered. Collections of different gravity waves would not display the separate characteristics of the individual components, and the possibility of strong interaction between atmospheric tides and gravity waves has been suggested from both meteor and chemical release data^(16,45) and apparently confirmed by the radar meteor studies of Spizzichino⁽³⁶⁾.

The purpose of this report is two fold: first to analyze the existing data in the 50 - 200 km range for irregular variations which could be due to

gravity waves, and secondly to determine methods of evaluating the effects of these observed irregular winds, densities, pressures, and temperatures on the stability, control, and dynamic heating of space craft such as the space shuttle vehicle. The following sections present results of measurements which establish the magnitude, statistics, and spatial and temporal structure of the irregular atmospheric variations. Section 7 of this report develops analytic methods, based on an analogy of the irregular motion field with axisymmetric turbulence, which allow measured or model correlations or structure functions to be used to evaluate the effective frequency spectra of scalar and vector quantities on a space craft moving at any speed and at any trajectory elevation angle.

2. DATA ANALYSIS INTERPRETATION

Structure Functions. An alternate form of the correlation function known as the structure function was first used extensively by Russian meteorologists in the analysis of turbulence. The structure function of a statistically stationary time varying process $f(t)$ is given by

$$D(\tau) = \langle [f(t + \tau) - f(t)]^2 \rangle \quad (1)$$

where the structure function D depends only on the time displacement τ because of the statistical stationarity. The angle brackets in (1) denote averaging.

Structure function analysis can be applied to wave phenomena also. Consider the process $f(t)$ to be a wave of frequency ω and amplitude A , i.e. $f(t) = A \sin(\omega t + \alpha)$, where α is a phase angle. If the averaging process is taken to be integration over any whole number of periods, where the period $T = 2\pi/\omega$, then the mean square value of $f(t)$ is $\langle f^2 \rangle = A^2/2$. It is also easy to determine that the structure function in this case is given by $D(\tau) = A^2 (1 - \cos \omega \tau)$. Thus the structure function of a single component wave field has the properties of being proportional to τ^2 for very small time displacements τ (since the leading term in $1 - \cos \omega \tau$ is $\omega^2 \tau^2/2$) and being periodic with the same frequency ω as the wave. Notice that the first maximum in $D(\tau)$ would occur at $\tau = \pi/\omega = T/2$, so the first maximum occurs at the half period value. The value of the maximum is $2A^2$.

The structure function analysis of waves can easily be extended to a set of waves which are part of a harmonic series. Consider $f(t)$ to be periodic with period T and to be made up of N different waves each wave n having a frequency $\omega_n = 2n\pi/T$, i.e.

$$f(t) = \sum A_n \sin(\omega_n t + \alpha_n) \quad (2)$$

where the summation is from $n = 1$ to $n = N$. Using the same type of averaging by integrating as on the single wave, one can determine that the mean square value of f is given by

$$\langle f^2 \rangle = \sum A_n^2 / 2 \quad (3)$$

and that the structure function is given by

$$D(\tau) = \sum A_n^2 (1 - \cos \omega_n \tau) \quad (4)$$

Thus again the behavior at small time displacement is proportional to τ^2 , since the leading term in (4) is $\sum A_n^2 \omega_n^2 \tau^2 / 2$. The structure function in this case is again periodic with period T and has components with amplitudes related to the square of the amplitudes of the corresponding frequencies in the process $f(t)$.

If the process $f(t)$ is made up of sufficient components that it must be considered as having a continuous spectrum of amplitudes $A(\omega)$ (as is the case with turbulence and may also be the case when gravity wave modes have significant nonlinear modal interaction) then $f(t)$ can be represented by

$$f(t) = \int_{-\infty}^{\infty} A(\omega) e^{i\omega t} d\omega \quad (5)$$

(For a more rigorous discussion of spectral representation see Lumley and Panofsky⁽⁴⁶⁾ and Lin⁽⁴⁷⁾). The mean square value of $f(t)$ is given by

$$\langle f^2 \rangle = 2 \int_{-\infty}^{\infty} \phi(\omega) d\omega \quad (6)$$

where $\phi(\omega)$ is the spectral density of the mean square variations of $f(t)$. The

structure function is given by

$$D(\tau) = 2 \int_0^\infty \phi(\omega) (1 - \cos \omega\tau) d\omega \quad (7)$$

Again the initial variation of $D(\tau)$ for small time displacements is proportional to τ^2 since

$$D(\tau) = [\int_0^\infty \omega^2 \phi(\omega) d\omega] \tau^2 \quad \tau \rightarrow 0 \quad (8)$$

However, at large time displacements $D(\tau)$ is not periodic but approaches a constant value of $2\langle f^2 \rangle$. This is seen readily from the fact that $D(\tau)$ is related to the correlation function $\rho(\tau)$ by

$$D(\tau) = 2\langle f^2 \rangle [1 - \rho(\tau)] \quad (9)$$

for all stationary processes $f(t)$. Hence, because $\rho(\tau)$ approaches 0 for large τ , then

$$D(\tau) = 2\langle f^2 \rangle \quad \tau \rightarrow \infty \quad (10)$$

In addition, if there is an appreciable range of frequencies over which $\phi(\omega)$ varies as a power law

$$\phi(\omega) = C \omega^{-a} \quad (11)$$

then there is a range of time displacements over which

$$D(\tau) \approx C \left[\int_0^\infty x^{-a} (1 - \cos x) dx \right] \tau^a - 1 \quad (12)$$

where $x = \omega\tau$ and the integral in brackets is some definite constant value.

Thus observed power law behavior of the structure function (i.e. $a - 1$) can be related to the power law of the spectral density (i.e. $-a$).

Daily Difference Analysis. A technique for resolving irregular variations in atmospheric winds or other parameters has been previously developed by Woodrum and Justus^(43,44) for application to chemical release data. This technique does not rely on explicit extraction of tides and prevailing values and does not require large amounts of data. Hence it is well suited for the study of irregular variations at high altitudes where data is limited in quantity.

As an example of the application of this technique consider two vertical profiles $F_1(z)$ and $F_2(z)$ of a parameter $F(z)$ where F might be a wind component, pressure, density, or temperature. Suppose that the two vertical profiles were measured at the same time of day and within a few days of each other. The assumption is made that the two profiles are represented at all measured heights z by the relations

$$\begin{aligned} F_1(z) &= F_o(z) + f_1(z) \\ F_2(z) &= F_o(z) + f_2(z) \end{aligned} \quad (13)$$

where $F_o(z)$ is a profile made up of the prevailing value, tidal variation, and any other diurnally repeating component of F . The profiles $f_1(z)$ and $f_2(z)$ are the profiles made up of the gravity wave components and any other non-diurnally repeating components such as planetary waves, synoptic variations, and variations of the tidal parameters from day-to-day. If the original data measuring technique did not filter out the turbulent components these would also appear as a contribution to $f_1(z)$ and $f_2(z)$, and if the number of days interval between the measured profiles becomes large then seasonal trends will also make a contribution. It is readily apparent from (13) that the difference in the measured values at any height z is equal to the difference in the irregular values at that height, i.e.

$$\Delta F(z) = F_2(z) - F_1(z) = f_2(z) - f_1(z) \quad (14)$$

Two further assumptions are now made: first that the irregular variations are statistically stationary and vertically homogeneous, and secondly that the irregular variations at the two measurement times are uncorrelated with each other. The second assumption is valid only if the irregular variations are made up of components whose periods are small compared to the interval between the measurements (e.g. gravity waves of up to a few hours period). If longer period phenomena, say planetary waves, of a predominate period of n days make a significant contribution then they should cause peaks in the average ΔF 's, at multiples of $n/2$ days. In the present analysis the ΔF 's are considered stationary. The analysis of chemical release winds⁽⁴⁴⁾ did not show significant variations of average ΔF 's with the number of days difference, and the study of this question for variations at lower altitudes will be the subject of later investigation.

Under the assumptions outlined above it can be shown that certain properties of the data difference values can be related to the irregular variations. For example consider an average (at the same altitude) over an "ensemble" of several profile pairs. The mean square difference is thus given by

$$\langle [\Delta F(z)]^2 \rangle = \langle f_2^2(z) \rangle + \langle f_1^2(z) \rangle - 2\langle f_1(z) f_2(z) \rangle = 2\langle f^2(z) \rangle \quad (15)$$

where the last step is possible because of the independence and stationarity of $f_1(z)$ and $f_2(z)$. The development leading to (15) is also taken as justification that the probability distribution of the data differences (divided by $\sqrt{2}$) is the same as the probability distribution of the irregular variations. However, this is strictly true only if the distribution is Gaussian.

The vertical structure function of the data differences is also related

to the structure function of the irregular variations. The vertical structure function of the data differences is given by

$$D_{\Delta F}(\zeta) = \langle [\Delta F(z + \zeta) - \Delta F(z)]^2 \rangle \quad (16)$$

where, again, the angle brackets represent an "ensemble" average. Substitution of (14) and rearrangement produces

$$\begin{aligned} D_{\Delta F}(\tau) &= \langle [f_2(z + \zeta) - f_2(z)]^2 \rangle + \langle [f_1(z + \zeta) - f_1(z)]^2 \rangle \\ &\quad - 2\langle [f_2(z + \zeta) - f_2(z)][f_1(z + \zeta) - f_1(z)] \rangle \end{aligned} \quad (17)$$

Application of the assumptions of independence and vertical homogeneity of the f 's results in

$$D_{\Delta F}(\tau) = 2\langle [f(z + \zeta) - f(z)]^2 \rangle = 2D_f(\zeta) \quad (18)$$

In other words, the vertical structure function of the data differences is twice the vertical structure function of the irregular variations.

In addition to vertical structure functions, horizontal structure functions were also calculated by differencing data from the up and down trail trajectories of rockets or from closely spaced simultaneous observations. It should be noted that the assumption of independence of the irregular variation profiles would not be valid in this case, however, and this type of difference therefore yields a structure function which has significant variation with the distance between the places of evaluation of the two profiles. However, since the effects of tides and other phenomena are not removed, the horizontal structure functions yield valid results on truly irregular variations only if the distance between profiles is kept small compared to the horizontal wave lengths of these tides and other phenomena. It should also be noted that the hori-

zontal structure function used for velocity is actually the structure function of the horizontal velocity magnitude

$$D(r) = \langle [u(\tilde{x} + r) - u(\tilde{x})]^2 \rangle + \langle [v(\tilde{x} + r) - v(\tilde{x})]^2 \rangle \quad (19)$$

where u is the eastward velocity component, v is the northward component, \tilde{x} is the horizontal vector location of one velocity evaluation, r is the vector displacement between the locations of velocity evaluation, and r is the magnitude of the vector r . The definition (19) is dependent on the magnitude r and not the direction of the displacement and no separate considerations of longitudinal and transverse structure functions are required. (A longitudinal structure function would be of the form $\langle [u^2(x + \Delta x) - u(x)]^2 \rangle$ and a transverse structure function would be of the form $\langle [u^2(y + \Delta y) - u(y)]^2 \rangle$.

Harmonic Analysis. In addition to a large irregular component, the winds and thermodynamic variables in the upper atmosphere are composed of regular variations produced by diurnal, semidiurnal, and other tidal components, and possibly long-period variations such as planetary waves. At the present time there is no method of resolving the values determined from a single profile into these various components. However, a series of profiles determined at a sequence of closely spaced times can be used to resolve the various components. A sequence of measured values at a given altitude are fit by a least squares process with the function

$$F(t) = A_0 + A_{12} \sin(2\pi t/12 + \phi_{12}) + A_{24} \sin(2\pi t/24 + \phi_{24}) \quad (20)$$

where the time t is measured in hours, A_0 is the mean value of the parameter, A_{12} and A_{24} are the amplitudes of the 12 hour, and 24 hour period tides, and

ϕ_{12} and ϕ_{24} are phase angles for those tidal components. The A's and ϕ 's are the parameters determined by the least squares process (indirectly by first evaluating coefficients of sine and cosine terms equivalent to (20)).

The computed tidal parameters were evaluated at each kilometer altitude point and were found to form smooth profiles of variation with altitude. After the mean values and tidal components have been determined from a series of profiles, then these values may be subtracted from the observed values to yield residual components. These residual values can be evaluated at each altitude for each of the profiles in the sequence and profiles of irregular variation values constructed. Each of these irregular parameter profiles can be used to evaluate vertical structure functions and values from different profiles in the time sequence can be differenced to computed time structure functions.

3. PROBABILITY DISTRIBUTIONS AND MAGNITUDES

Distribution Statistics. The probability distribution $p(f)$ of a parameter $f(x, t)$ is defined so that $p(f_o) df$ is the probability of observing a value of the parameter with a value between f_o and $f_o + df$. The usual normalization is to unit probability for observing a value of f in the range $-\infty$ to $+\infty$. This is expressed mathematically by the relation

$$\int_{-\infty}^{\infty} p(f) df = 1 \quad (21)$$

The average value of f is found by the equation

$$\bar{f} = \langle f \rangle = \int_{-\infty}^{\infty} f p(f) df \quad (22)$$

and the probability distribution function can be characterized by the moments μ_k about the average. The moments are given by

$$\mu_k = \langle (f - \bar{f})^k \rangle = \int_{-\infty}^{\infty} (f - \bar{f})^k p(f) df \quad (23)$$

Of particular interest are the standard deviation σ , the skewness α , and the kurtosis β which are defined by

$$\begin{aligned} \sigma^2 &= \mu_2 \\ \alpha &= \mu_3 / \sigma^3 \\ \beta &= \mu_4 / \sigma_4 \end{aligned} \quad (24)$$

The Gaussian probability distribution is given by

$$p(f) = \exp[-(f - \bar{f})^2 / 2\sigma^2] / (2\pi)^{1/2} \sigma \quad (25)$$

and is thus completely characterized by its mean value and standard deviation.

The skewness (as with all odd moments) for the Gaussian distribution is zero.

The kurtosis for the Gaussian distribution is 3.

Characteristics of the probability distribution of irregular winds at chemical release altitudes have been reported by Justus⁽⁴⁴⁾. For this study data on winds, pressures, densities, and temperatures were gathered from a large number of sources and analyzed in the same fashion, (i.e. as outlined in Section 2). These included the Meteorological Rocket Network (MRN) data for the years 1964 - 1969⁽⁴⁸⁾; NASA Goddard grenade and pitot tube data for 1960 - 1969⁽⁴⁹⁾; chemical release winds from Eglin AFB, Florida 1962 - 1971⁽⁵⁰⁾, from Barbados and Yuma⁽⁵¹⁾, Wallops and other locations⁽⁵²⁾; ROBIN falling sphere data⁽⁵³⁾, and other rocket and falling sphere data⁽⁵⁴⁾. In addition to these collected data, individual data sets from many sources were added to the computed probability distributions^(19,20,54-61). These data include satellite measurements, meteor winds, and ion probe observations.

Figures 1 through 5 show some representative results of the probability distribution analysis. The ordinates of these graphs are the number of observed values. Bars forming the shaded area represent the observed values and the large dots are the expected number based on zero mean and the observed standard deviation in a Gaussian distribution. Relative probabilities may be obtained by dividing the number of observations by the total number observed, given on each graph. The abscissa on the velocity plots, Figure 1 and 2, are the equivalent irregular wind magnitudes determined by the observed data value velocity differences divided by the square root of two (cf. equation (15)). For pressure, density, and temperature distributions the abscissas are relative fluctuation magnitudes i.e. p'/p_o , ρ'/ρ_o , T'/T_o where the fluctuation values are determined by the observed data differences divided by $\sqrt{2}$.

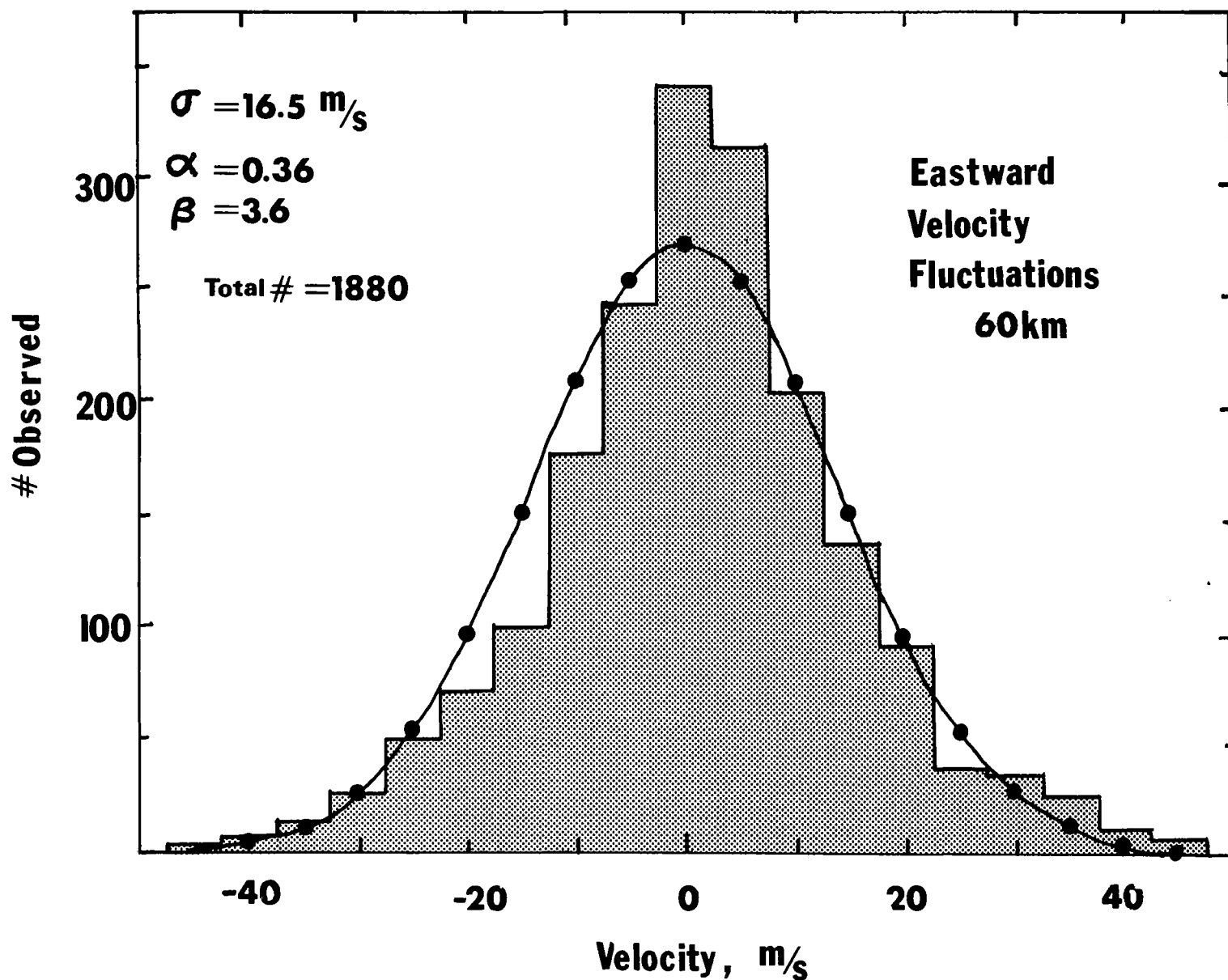


Figure 1. Distribution of the eastward component 1969 MRN irregular winds in the 55 to 65 km height range.

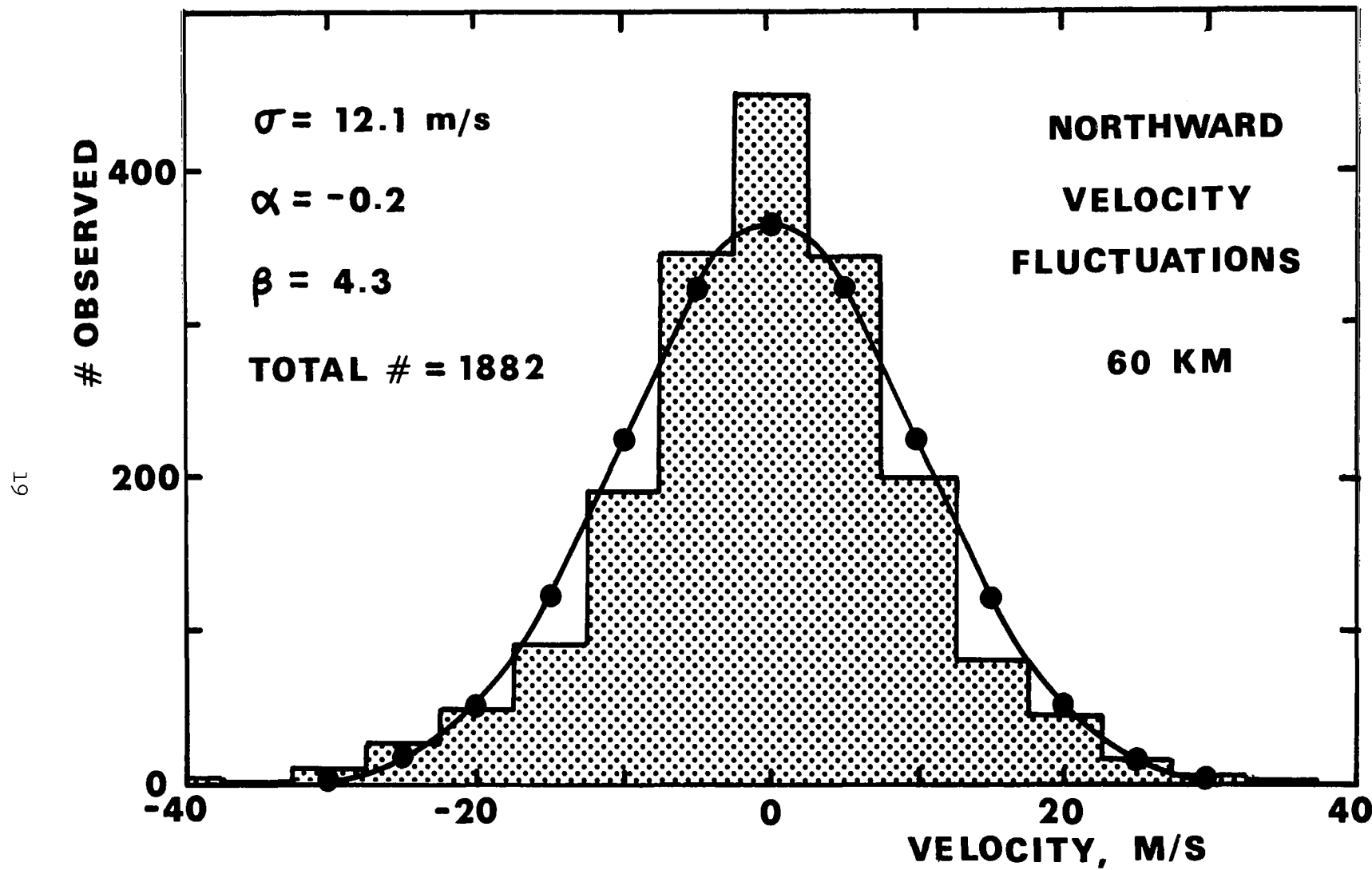


Figure 2. Distribution of the northward component 1969 MRN irregular winds in the 55 to 65 km height range.

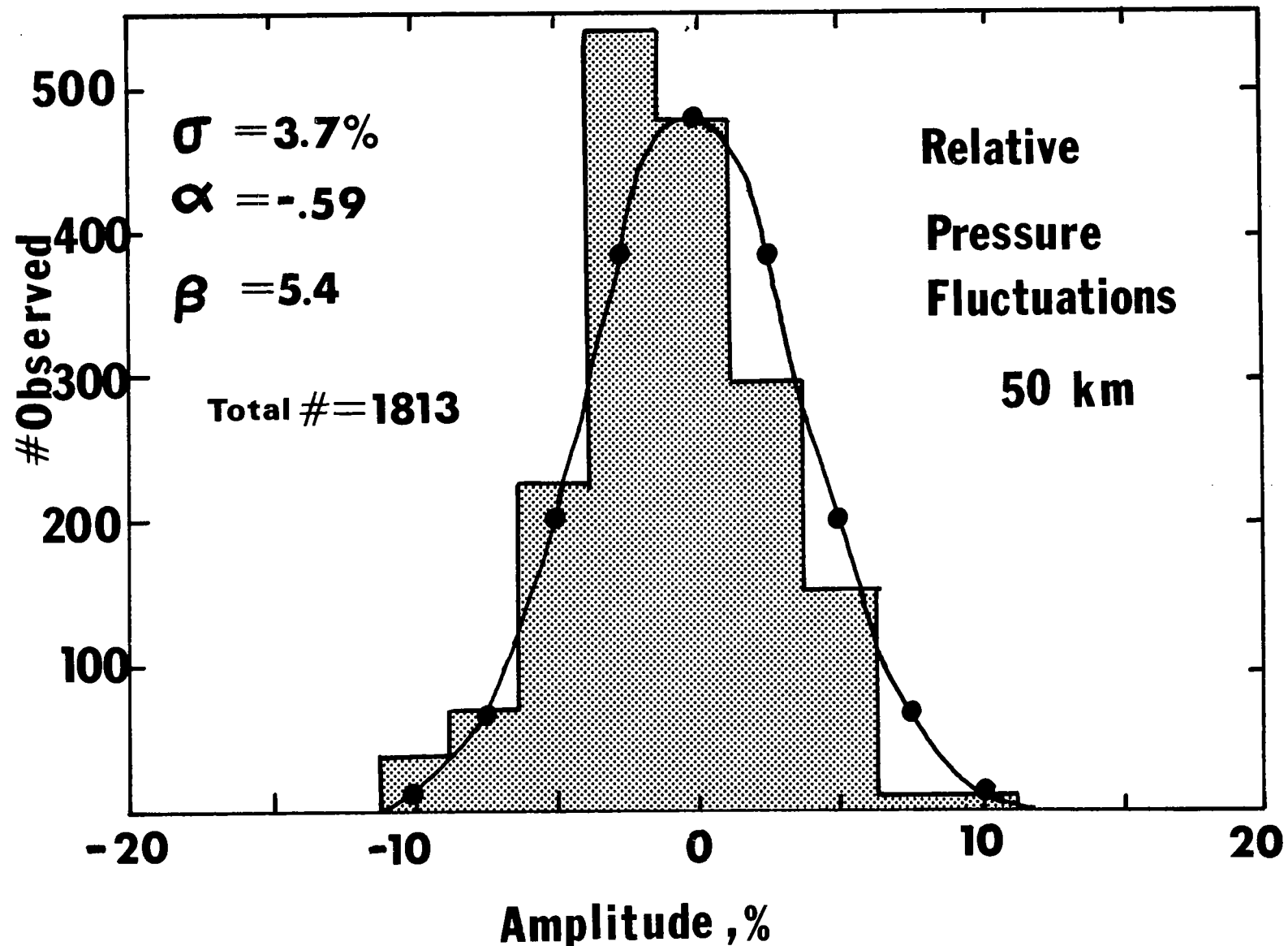


Figure 3. Distribution of the 1969 MRN relative pressure fluctuations p'/p_0 in the 45 to 55 km height range.

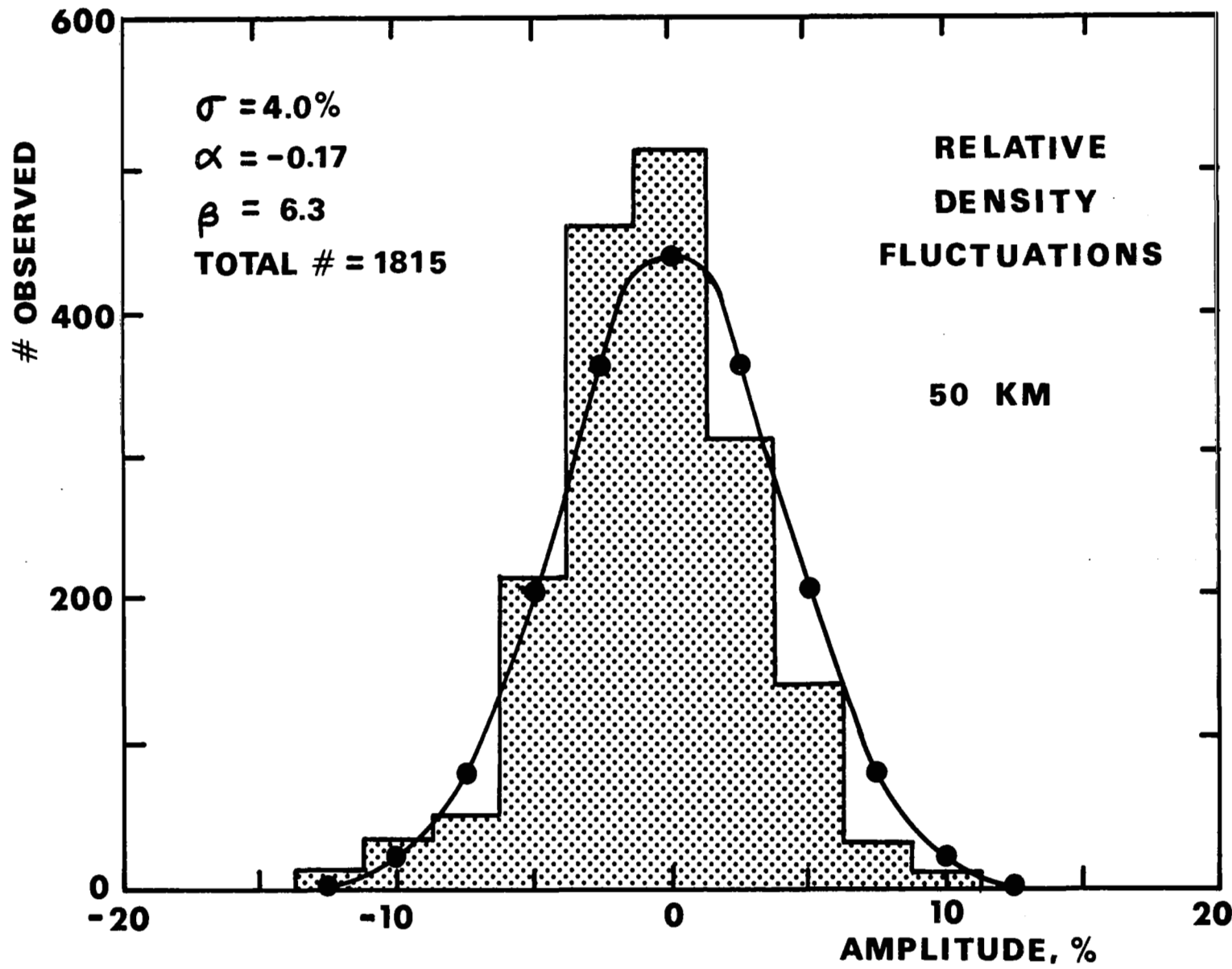


Figure 4. Distribution of the 1969 MRN relative density fluctuations ρ / ρ_0 in in the 45 to 55 km height range.

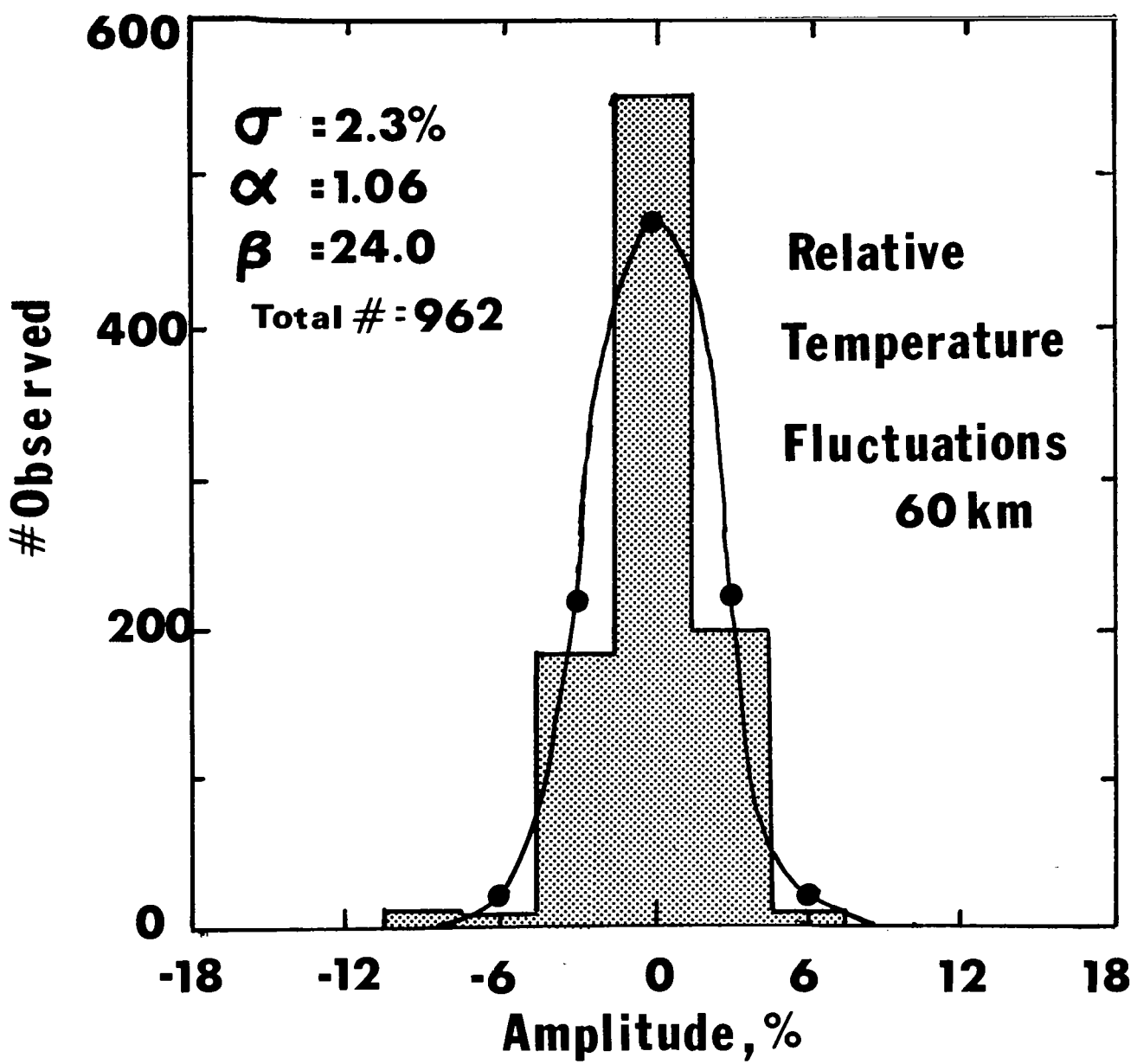


Figure 5. Distribution of the 1969 MRN relative temperature fluctuations T/T_0 in the 55 to 65 km height range.

$$\begin{aligned}
 p' &= (p_2 - p_1)/\sqrt{2} \\
 \rho' &= (\rho_2 - \rho_1)/\sqrt{2} \\
 T' &= (T_2 - T_1)/\sqrt{2}
 \end{aligned} \tag{26}$$

and the mean values are determined by the average of the observed data values

$$\begin{aligned}
 p_o &= (p_1 + p_2)/2 \\
 \rho_o &= (\rho_1 + \rho_2)/2 \\
 T_o &= (T_1 + T_2)/2
 \end{aligned} \tag{27}$$

The observed magnitudes, as characterized by the standard deviations of the distributions, showed latitude and altitude variations which are discussed later in this section. The computed values of skewness parameter α showed no variation with height or latitude. Values computed for the kurtosis β did show a significant altitude variation discussed below. Table 4 shows a summary of the calculated α values for the irregular winds, pressure, density, and temperature. The values of σ , α , and β were computed from the observed distribution in histogram form, with Sheppard's corrections applied, rather than from each individual observed value. In order to test the significance of the deviations of α from the expected Gaussian value of zero the test explained by Keeping⁽⁶²⁾ was employed. The value used in the test for the number of data was the estimated number of independent data values rather than the total number observed. The number of independent values is less than the total for two reasons. First the data values at adjacent 1 km height intervals are not independent but are correlated with each other, and secondly if a set of data from n consecutive days are to be differenced then $n(n - 1)/2$ differences can be formed, but only $n - 1$ of these differences are independent of each other.

Table 4. Average Skewness α of
the Probability Distribution of the
Irregular Variation

Irregular Variation Parameter	Total Number of Observations	Number of Independent Observations	α
p'	4175	1252	-0.11
ρ'	4151	1252	-0.09
T'	4413	1432	-0.22*
u (eastward)	9559	2359	+0.13*
v (northward)	9078	2283	-0.10*

* Values which are significantly different (at the 1% level) from the zero value expected for a Gaussian distribution. Significance tests are those given by Keeping⁽⁶²⁾ and based on the number of independent observations.

To account for the correlation over height it was assumed that data values separated by 5 km of altitude could be taken as independent for purposes of computing the number of independent observations.

Three of the skewness values in Table 4 were computed to be significantly different from zero. A positive α indicates an excess of large positive values and a deficit of large negative values compared to a symmetric distribution. The reverse of this would be true for a negative α . The largest magnitude skewness is for the irregular temperature distribution. Because of the small σ of the temperature there were few intervals into which the values fell and the histogram technique, even with Sheppard's corrections, probably does not accurately estimate the higher moments. Of the two remaining α 's which are significantly different from zero, one is positive and the other negative. Therefore, it is not clear what if any significance should in fact be placed on these skewness results.

The values computed for the kurtosis β showed a significant altitude variation, as reflected in Figure 6. The dotted area represents the approximate range within which β would not be significantly different from the expected Gaussian value of 3. The notation used in Figure 6 is u for the eastward wind component and v for the northward wind component. The values are consistently high-to-normal below 100 km and low-to-normal above 100 km. The extremely large values found for the irregular temperature may be due to the same problem of low σ and small number of intervals, which also led to high magnitudes for the skewness.

High values of β indicate a distribution with a high central peak and broad "skirts". A low β indicates the reverse of this. The height variation of β is consistent with the previous measurements by Justus⁽⁴⁴⁾ of low β for

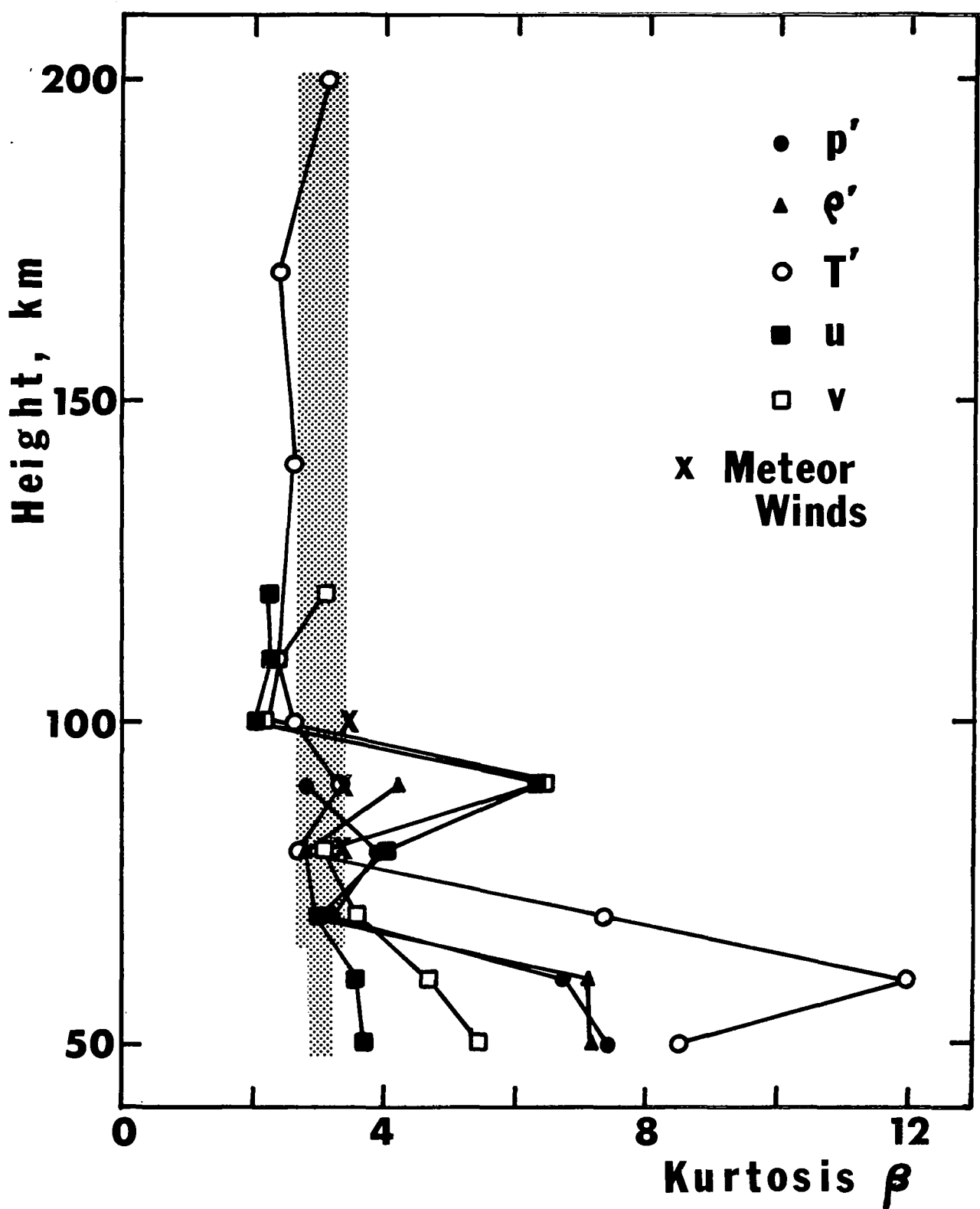


Figure 6. Height variation of the kurtosis β of the distributions of the irregular winds, pressure, density, and temperature. u is the eastward wind component and v is the northward component.

the irregular winds, because they were for the region near 100 km where low β values are indicated. Also shown on Figure 6 are the β values of the distributions of irregular winds determined as residual winds from meteor data from Garchy, France⁽⁵⁸⁾ and Durham, New Hampshire⁽⁵⁹⁾ after resolution of the tidal winds by a data reduction method developed by Groves⁽⁶³⁾. The meteor data indicate near Gaussian values for β in the 80 - 100 km region, in slight disagreement with the other data, but in good agreement with Russian meteor results computed by Pokrovskiy, et al.⁽⁶⁴⁾.

The high β values of the MRN data at 50 - 60 km persisted even when the data was devided by site location. The β values computed for each site separately and then averaged were approximately the same as those plotted in Figure 6, except for the relative temperature fluctuations. The site averaged β of the T'/T_0 distribution was 6.06 at 50 km and 9.34 at 60 km, somewhat lower than the values of Figure 6.

Magnitude Variation with Height. The magnitude of the irregular variations, as represented by the standard deviation σ of the probability distribution, showed significant height variation. The measured height variation of the irregular winds is seen in Figure 7. The data which went into Figure 7 included the 1969 MRN data from 8 sites: Fort Sherman, Cape Kennedy, Ascension Island, White Sands, Fort Greeley, Point Mugu, Barking Sands, and Fort Churchill, plus all of the data from other sources. The magnitude determined by the daily difference method from the MRN and other data are shown by the data points connected by solid and dashed curves. In Figure 7, as elsewhere, u is the eastward wind component and v is the northward component. At 50 and 60 km the irregular winds are definitely anisotropic, with the eastward component dominating. At 70 km and above no significant anisotropy exists. In view of the

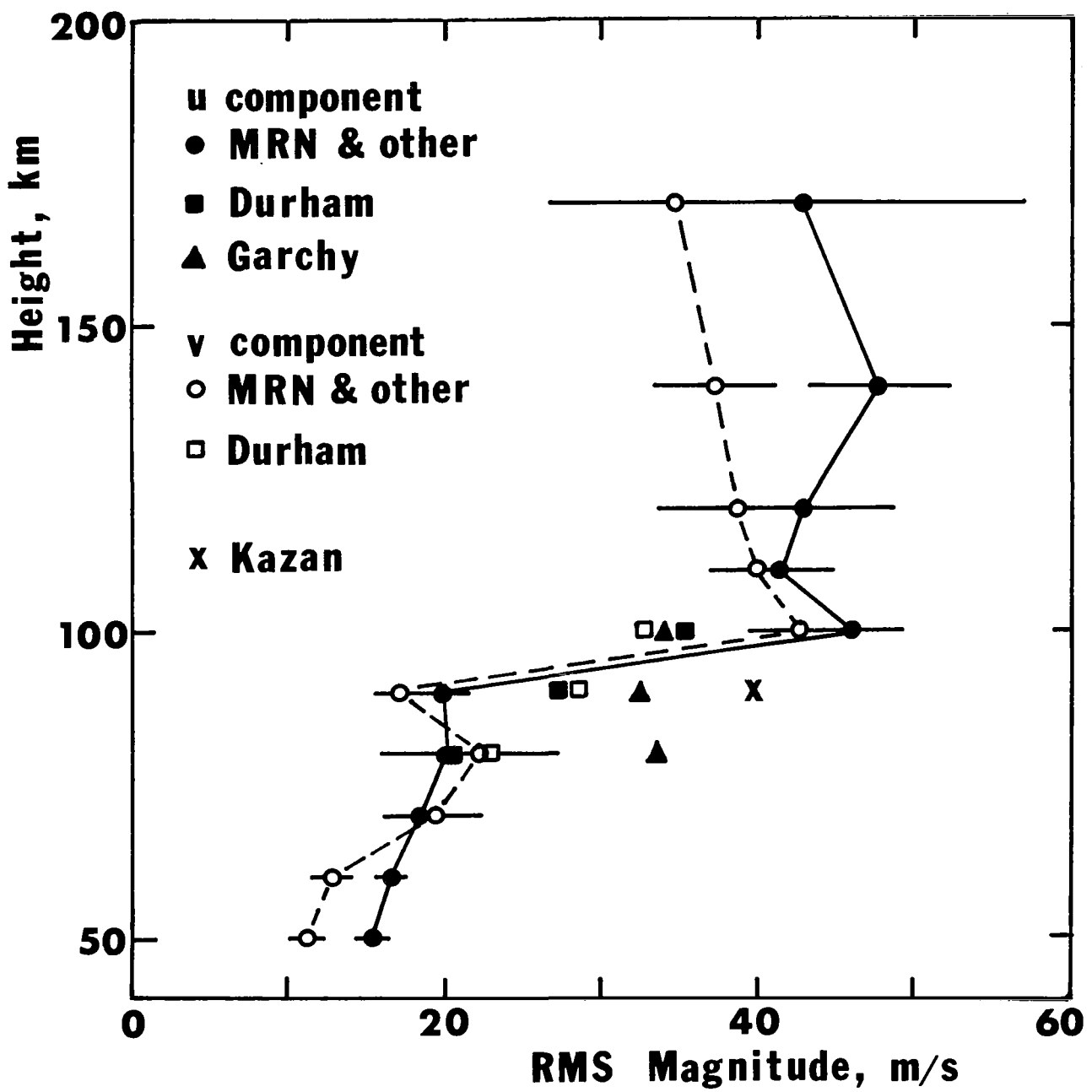


Figure 7. Height variation of the magnitude of the irregular winds. u is the eastward wind component and v is the northward component.

size of the error bars above 120 km, the apparent dominance of the eastward component at those heights is not considered to be significant. The increase of irregular wind magnitude with height is rather sharp between 90 and 100 km as measured by the daily difference data. A rapid though not quite so sharp increase at these altitudes is also seen from the Durham meteor data irregular winds. Although the Garchy data agrees in general magnitude, the sharp rate of increase near 90 km does not appear in the Garchy meteor data. A still different value near 90 km was obtained from Russian meteor winds from Kazan⁽⁶⁴⁾. The Kazan value appears to be more representative of the higher altitude data than the Durham or Garchy data. These variations lead one to conclude that the height variation curve of Figure 7 given by the MRN and other data may be valid in detail only for the North American continent.

Linearized gravity wave theory with no dissipation predicts⁽¹⁾ that the gravity wave kinetic energy density $\rho_0 \langle u^2 + v^2 \rangle$ remains constant with height. It is obvious from Figure 7 that considerable dissipation takes place above 100 km since the irregular wind magnitude remains relatively constant while the atmospheric density ρ_0 decreases rapidly. However, significant dissipation also occurs between 50 and 100 km despite the increasing irregular wind magnitude. For example, the density decreases by a factor of about 5×10^{-4} from 50 to 100 km while the mean square irregular velocity increases by a factor of only about 8.

The height variation of the irregular pressure, density, and temperature is shown in Figure 8. The data are expressed as variations relative to the mean atmospheric parameters. The declining values above 110 km confirm the fact that significant dissipation of the irregular variations occurs above about 110 km. The dissipation above 100 km is not unexpected in view of

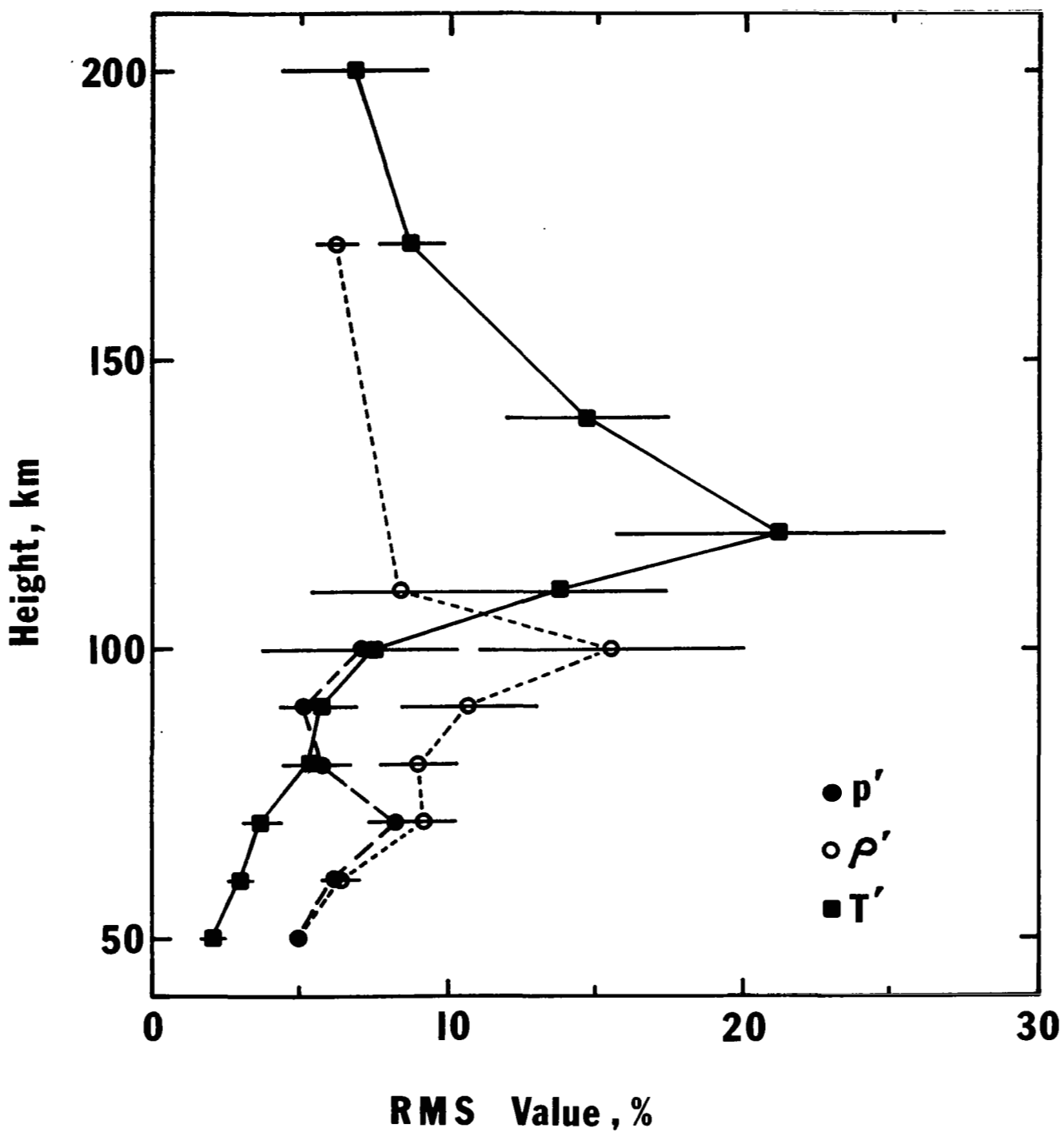


Figure 8. Height variation of the magnitude of the relative pressure p'/p_0 , density ρ'/ρ_0 , and temperature T'/T_0 .

earlier theoretical work on the dissipation of gravity waves^(3,65) and experimental observations of the height variation of irregular winds^(43,44) in this region. However the more-or-less continuous dissipation from 50 to 100 km is somewhat unexpected.

Figure 8 shows that the relative temperature variation magnitude between 50 and 70 km is significantly smaller than for the relative pressure or density, which are about equal. Between 80 and 100 km the relative pressure and temperature variation magnitudes becomes about equal and smaller than the relative density variations. Above 100 km the relative density variations become smaller than those for the relative temperature.

At first one might think that the Boussinesq approximation should apply to the pressure, density, and temperature variations and hence that the relative pressure variations should be much smaller than the relative density and temperature. However, as shown by Dutton and Fichtl⁽⁶⁶⁾, for motions of vertical scale not small compared to the scale height, the magnitudes of all three parameters are comparable. It will be shown later that the vertical scales are comparable with the scale height. Therefore, the relative values of the irregular thermodynamic parameters are related by

$$\frac{p'}{p_o} = \frac{\rho'}{\rho_o} + \frac{T'}{T_o} \quad (28)$$

and in the mean square they would be related by

$$\begin{aligned} \langle \left(\frac{p'}{p_o} \right)^2 \rangle &= \langle \left(\frac{\rho'}{\rho_o} \right)^2 \rangle + \langle \left(\frac{T'}{T_o} \right)^2 \rangle \\ &+ 2 \langle \left(\frac{\rho'}{\rho_o} \right) \left(\frac{T'}{T_o} \right) \rangle \end{aligned} \quad (29)$$

where the last term is basically the correlation between the density and temperature variations, which in the case of a single component wave train would

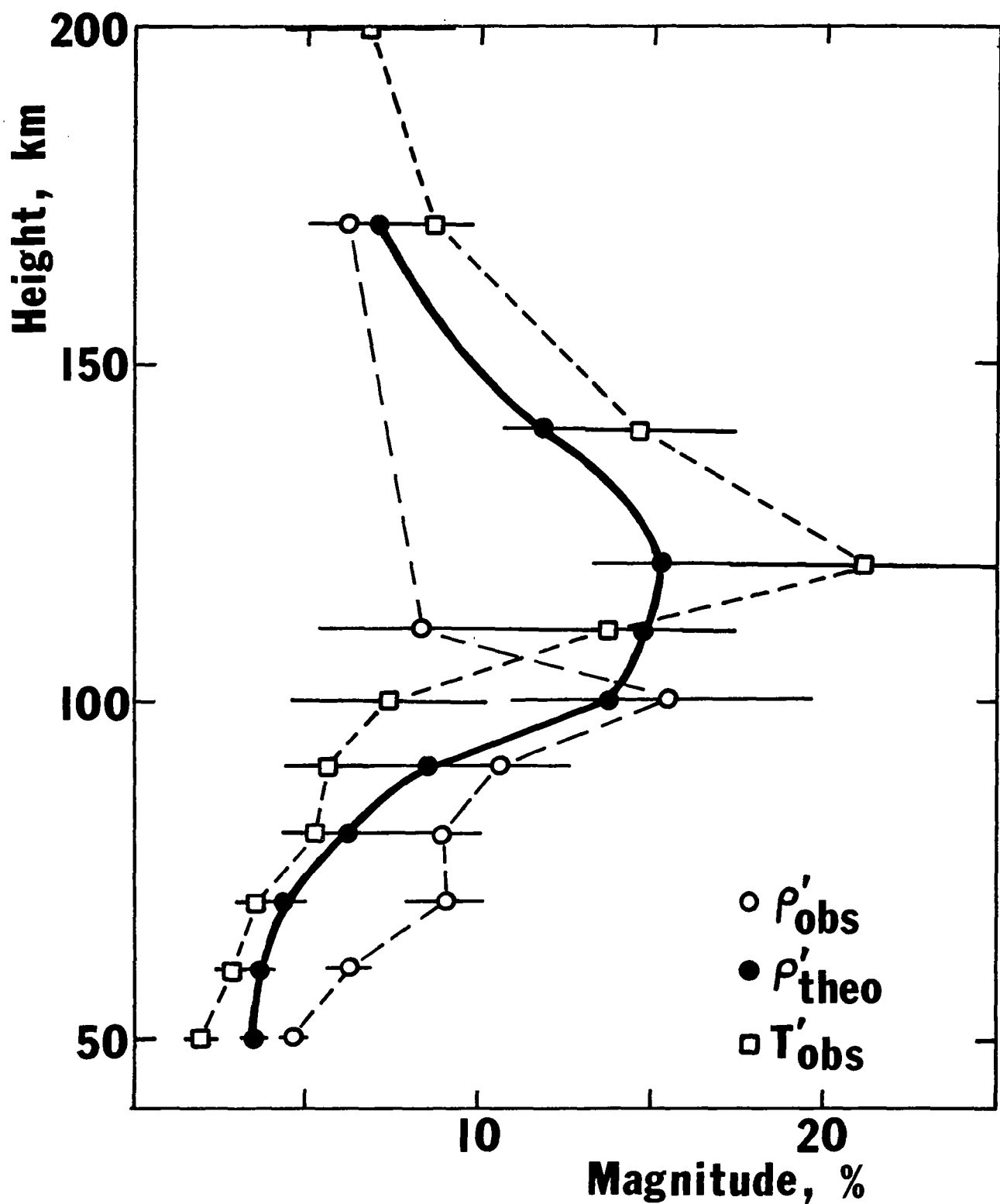


Figure 9. Comparison of observed height variation of ρ'/ρ_0 and T'/T_0 with Miller's (67) theoretical curve of ρ'/ρ_0 based on measured irregular wind magnitudes.

be dependent on the relative phase between the density and temperature wave variation. The changes discussed above in the relative magnitudes of the thermodynamic variables of Figure 8 therefore indicate a changing phase relationship with height. This changing phase relationship could be due to non-linear intermodal interactions or to selective model absorption of a complex gravity wave field. In either case it would be difficult to justify the changing relative magnitudes with the assumption of a simple mode gravity wave field.

A comparison of the height variation of the irregular winds and irregular density shown in Figure 9 gives good agreement with a theory developed by Miller⁽⁶⁷⁾, which predicts relative density variations proportional to rms velocity variation by a factor which varies with height. The theoretical values of ρ'/ρ_0 are related to the mean square irregular winds by the formula

$$|\rho'/\rho_0| = \{ [(\gamma - 1)/c^2 + (1/gT_0) dT_0/dz] \langle u^2 + v^2 \rangle \}^{1/2} \quad (30)$$

The U.S. Standard Atmosphere of 1962 was used to evaluate the speed of sound c , the acceleration of gravity g , the temperature T_0 and its height gradient dT_0/dz . The ratio of specific heats γ was assumed to be constant at a value of 1.4. The agreement between the observed ρ'/ρ_0 variation and that predicted by the theoretical formula is remarkably good, considering the uncertainties introduced by the use of standard atmosphere values. However, it does appear from the results shown in Figure 9 that the theoretical formula corresponds more nearly with the magnitude of the irregular temperature T'/T_0 than the density ρ'/ρ_0 .

Magnitude Variation with Latitude. Only the Meteorological Rocket Network data were available in sufficient quantity to study latitudinal variations.

The data which were used are 1964 - 1969 results from the MRN sites listed in Table 5. The average magnitudes, as determined from the daily difference method standard deviation of the distribution, are plotted in Figure 10 as a function of the observing station latitude. The curves identified as P and T are relative pressure p'/p_o and relative temperature T'/T_o in percent. The latitude variation of the relative density was essentially identical with that for relative pressure. The irregular velocity magnitudes are identified as U for eastward component and V for the northward component.

At both altitude levels in Figure 10 the relative temperature variation magnitudes are considerably smaller than the relative pressure or density. This is in keeping with the results previously shown in Figure 7. The magnitudes of the relative temperature variations are so small (1 - 2%) that one at first questions the validity of the interpretation that these represent atmospheric variations and not just observational error. First it should be pointed out that the daily difference method involves observations at the same time of day and therefore extraneous variation due to radiation errors⁽⁶⁸⁾ from measurements at different solar elevations cannot be a source of error. Secondly results of the study of rocketsonde repeatability⁽⁶⁹⁾ indicate temperature measurement accuracy of about 1°C which at 50 - 60 km is about 0.4% (velocity accuracy is estimated at about 3 m/s). Thus the observed relative temperature variation magnitudes of Figure 10 are between 2.5 and 5 times larger than the observational limit. Thirdly, the trend of increasing magnitude of variation with increasing latitude is consistent with the observed increased variability of the atmosphere at high latitudes⁽⁷⁰⁾ while it would be difficult to explain an increasing observational error with increasing latitude.

The general trend of increase with latitude is seen in all of the varia-

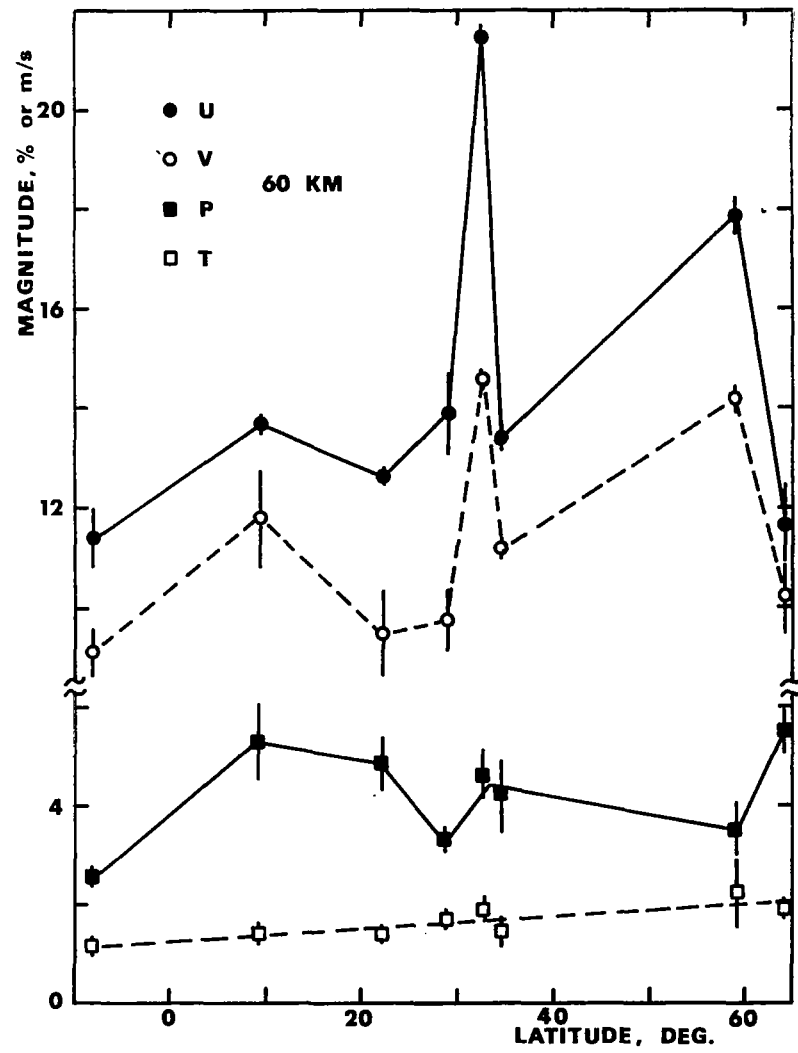
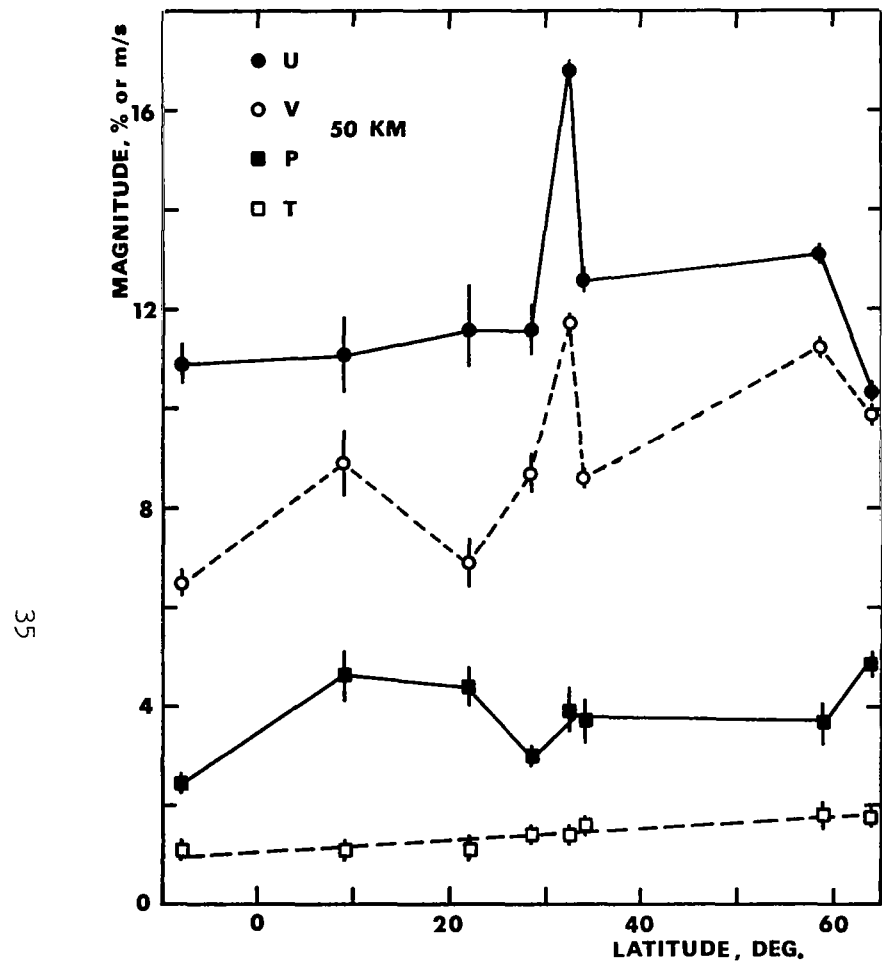


Figure 10. Latitude variation of the magnitude of the irregular winds and relative pressure and temperature. u is the eastward wind component and v is the northward.

TABLE 5. MRN SITE LOCATIONS

<u>Site Name</u>	<u>Latitude</u>	<u>Longitude</u>
Ascension Island, A.F.B.	7° 59' S	14° 25' W
Fort Sherman, Canal Zone	9° 20' N	79° 59' W
Barking Sands, Hawaii	22° 02' N	159° 47' W
Cape Kennedy, Florida	28° 27' N	80° 32' W
White Sands, New Mexico	32° 23' N	106° 29' W
Point Mugu, California	34° 23' N	119° 07' W
Fort Churchill, Canada	58° 44' N	93° 49' W
Fort Greely, Alaska	64° 00' N	145° 44' W

bles plotted in Figure 10. Two Exceptions to the trend are the sharp peak at 32.5° N latitude (the White Sands site), and the sharp drop in the 60 km data at 64° N latitude (the Fort Greely site). In an attempt to discover a possible cause for the peak value from the White Sands results a possible geographical cause was noted in the topography west of White Sands. Figure 11 shows several southwestern states and the upper portion of Mexico. The location of White Sands is labeled A. The shaded area shows the approximate region which is fairly densely populated with mountains with peak height of approximately 2 km or higher. The western portion of this area is made up of the Sierra Nevada Mountain Range, the middle portion is the Colorado Plateau Area and the Eastern section is a portion of the Rocky Mountains. Some peaks in the Sierra Nevada Range are identified in Figure 11: B is Mt. Whitney (4418 m), C is Toro Peak (2653 m), D is Mt. Palomar (1867 m), E is Santa Catalina (3089 m). Immediately East of the Sierra Nevadas is an area which is at or below sea level: F identifies Death Valley (-86 m), G is the Salton Sea (-72 m), and H is the Gulf of California. Any wind blowing toward White Sands from the WNW, W, or WSW would encounter this mountain-followed-by-lowlands terrain. Since White Sands is approximately 1000 km from the Sierra Nevada Range, then the dominant period of waves launched by those mountains reaching 50 - 60 km height at the location of White Sands should have periods near 150 min. or longer i.e. slightly more than two hours. This result was calculated using the method employed by Hines⁽⁷¹⁾ on gravity waves generated by nuclear explosions. This value is in general agreement with the periods of waves inferred later in the report from time structure function analysis. The reason why the Fort Greely values, especially at 60 km, are low is not clear at this time. However, the results of Theon et al.⁽⁷²⁾ have shown that wave structure evident in the 40 - 90 km

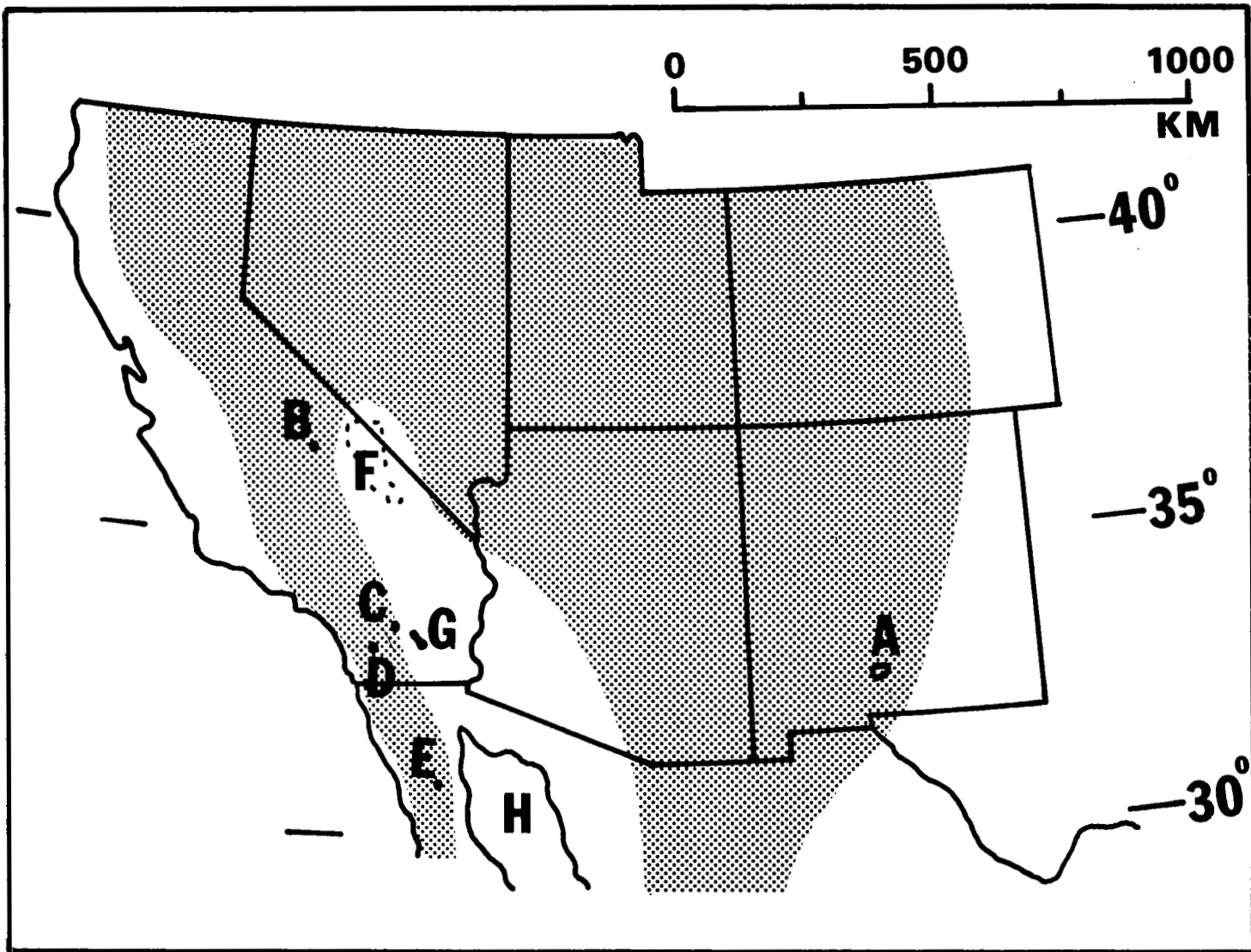


Figure 11. The location of White Sands (A) and the surrounding geography.

region over Pt. Barrow (71° N) in the winter (January - February) is entirely absent in the summer (June - August). This result indicates strong seasonal variation in the magnitude of upper atmospheric waves at high latitudes, possibly due to variation in the propagation characteristics of the atmosphere between the ground level and 40 km.

4. VERTICAL STRUCTURE FUNCTION DATA

The vertical structure function is defined as

$$D(\zeta) = \langle [V(z) - V(z + \zeta)]^2 \rangle \quad (31)$$

where V may be velocity component, pressure, temperature or density, z is the height coordinate and ζ is the height displacement.

Data. Profiles of residual winds, pressure, temperature and density were obtained from Meteorological Rocket Network Data by differencing pairs of wind, pressure, temperature, and density profiles according to the method discussed in section 2 (see equation (15)). The pair members were chosen such that both profiles occurred within ten minutes of the same local time of day and not more than fifteen days apart. This procedure was performed on data from the eight locations listed in Table 5. The time coverage of the data ranged from 1964 to 1971 and the height range was from 45 km to about 65 or 70 km.

In addition, similar profiles or residual winds were obtained from chemical release wind data taken at Eglin AFB in Florida⁽⁵⁰⁾, GCA data⁽⁵²⁾ and gun probe data from Barbados and Yuma⁽⁵¹⁾. The time coverage of this data was from 1959 to 1971 and the height range was from about 80 km to 140 km. The chemical release data also includes some vertical winds which were used in the vertical structure analysis^(50,73,74).

The ROBIN falling-sphere data taken at Eglin AFB on May 9 - 10, 1961, was used also⁽⁵³⁾. The height range of this data was from about 45 to 65 km. Irregular winds were also obtained from the ROBIN data by subtracting the tidal components determined by harmonic analysis from the raw data.

Analysis. The vertical structure functions of the residual winds were

computed for each residual wind profile by taking differences between values from the profile at altitudes different by the displacement amount and averaging over the profile. Similar analysis was performed for the pressure, temperature, and density data.

The MRN data were divided into groups according to the site location from which the data were taken, and data from each site was analyzed separately. Representative profiles of the vertical structure functions of these data are shown in Figures 12 and 13. At first the residual profiles from a particular site were divided into two height groups of 45 to 55 km and 55 to 65 km, and a structure function was calculated for each height group. However, the structure functions for the two groups were not significantly different; and thus, the height groups were recombined into one group.

Figure 12 shows the structure function for two profiles of residual north-south winds and two profiles of residual east-west winds. All four functions show the same general characteristics. For small vertical displacements the structure function increases approximately linearly on log-log scale and then levels off. A power law of the form $D(\zeta) = \text{const. } (\zeta)^n$ was fitted to each of the vertical structure functions of the MRN data over small vertical displacements ζ . The averages of the corresponding exponents n were 1.06 for the residual north-south winds and 0.94 for the east-west winds.

The average leveling-off values of the structure functions were found to be $197 \text{ m}^2/\text{sec}^2$ for the residual north-south winds, corresponding to $\sigma_n \approx 10 \text{ m/sec}$, and $237 \text{ m}^2/\text{sec}^2$ for the residual east-west winds, corresponding to $\sigma_e \approx 11 \text{ m/sec}$, in reasonable agreement with the values at 50 and 60 km in Figure 7.

Also, characteristic with most of the vertical structure functions was

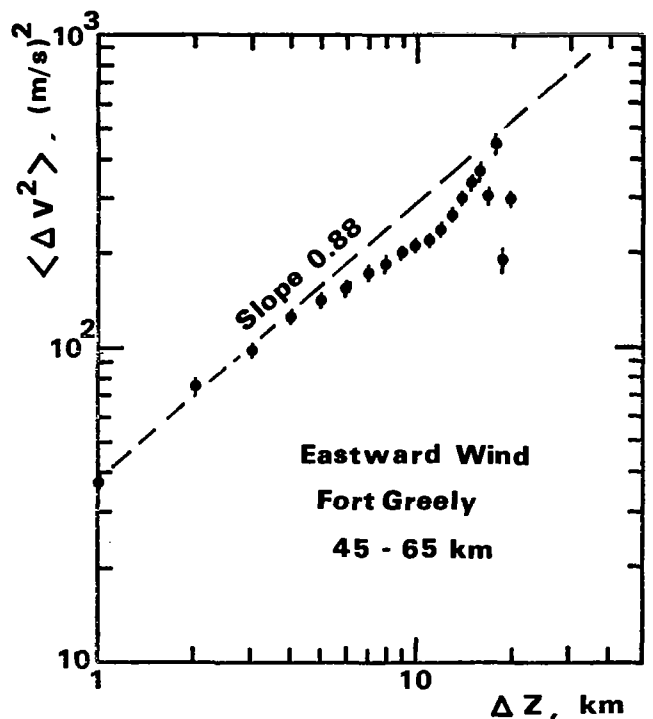
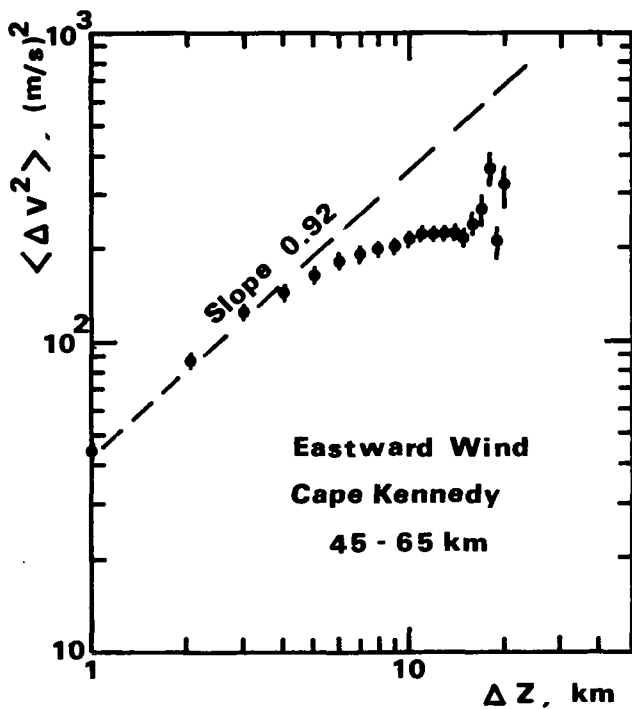
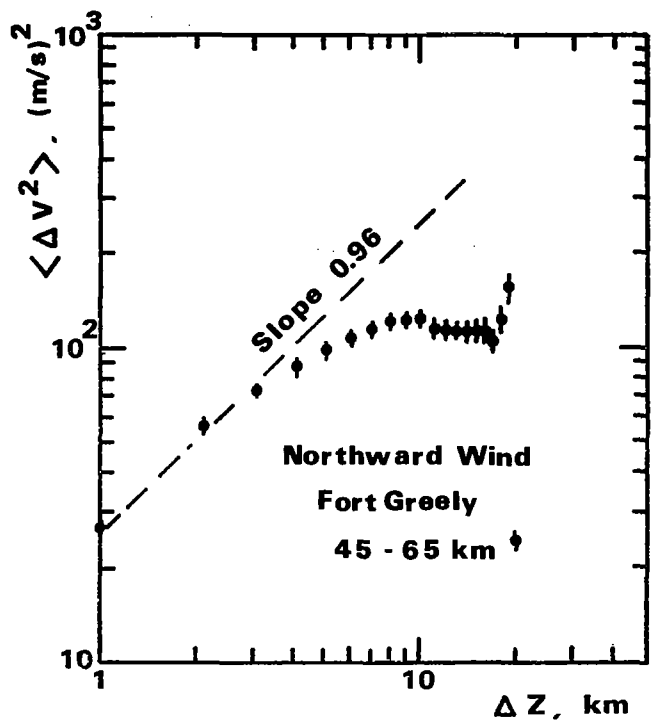
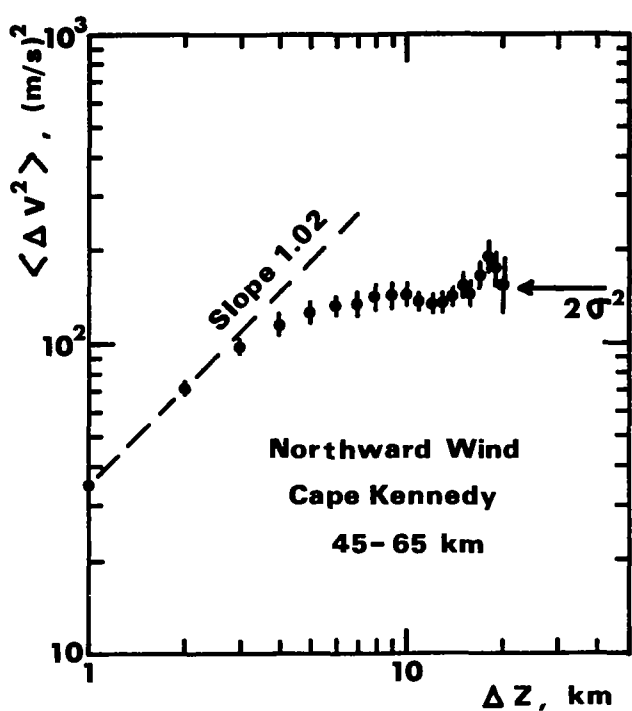


Figure 12. Vertical structure functions of MRN irregular wind data determined by the daily difference method.

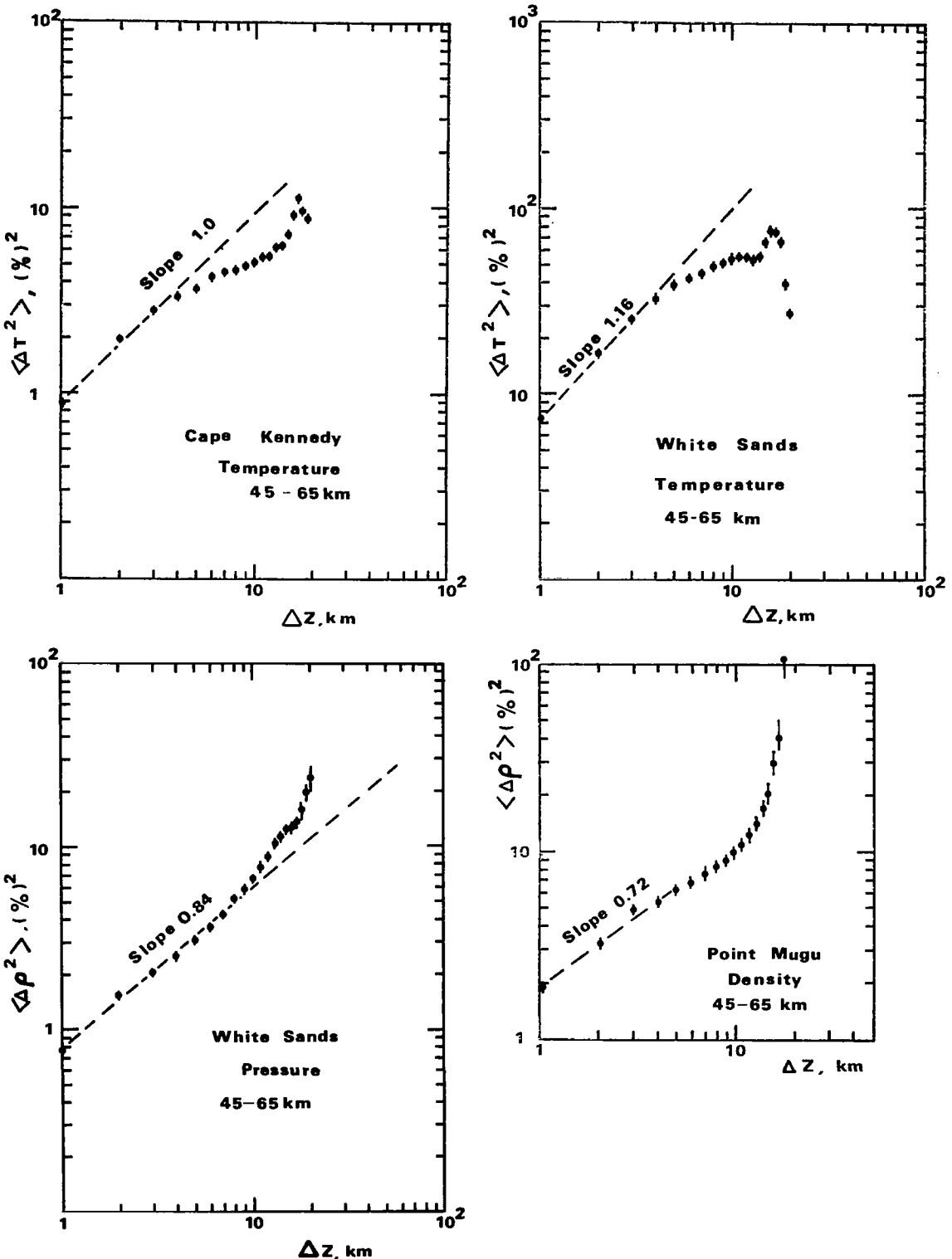


Figure 13. Vertical structure functions of MRN relative temperature, pressure, and density variations determined by the daily difference method.

the additional peak for a vertical displacement of about 18 km. This peak could be caused by a wave motion with a dominant vertical wavelength of about 36 km. The amplitude of this motion seems to vary from about 5 to 10 m/sec.

The horizontal arrow in the graph of the structure function for the northward winds at the Cape Kennedy site gives an example of the position of the leveling-off point ($2\sigma^2$) which was calculated from the daily-difference analysis. Actually, the daily-difference analysis calculates an average for the leveling-off value and would include the peak in the average. Thus, the value of $2\sigma^2$ calculated from the daily-difference program should be slightly larger than the value calculated from the vertical structure functions as is shown.

Figure 13 shows the vertical structure functions for two profiles of relative temperature deviation and one profile each of relative pressure and density deviation. The function for the temperature seems to behave similarly to the structure functions for the wind components in Figure 12. However, the vertical structure functions for the pressure and density have entirely different detailed characteristics. They do seem to have a linear log-log increase for small vertical displacements, but they have no leveling-off point. Some of the functions seem to peak at vertical displacements of 18 or 19 km similar to the peaks observed in the velocity structure functions whereas others continue to increase out to 20 km, the largest displacement calculated.

A power law $D(\zeta) = \text{const. } (\zeta)^n$ was fitted to the vertical structure functions for the temperature, pressure, and density data over small vertical displacements. The averages of the exponent n are 0.82, 1.09, and 0.65 for the pressure, temperature, and density respectively. The average leveling-off value of the temperature is $5.0(\%)^2$ corresponding to $\sigma = 1.6\%$, again in good agreement with previous results in Figure 8.

Figure 14 shows the vertical structure functions for the chemical release wind data. These data were broken into two height intervals, 80 to 110 km and 110 to 140 km. The functions show a linear log-log increase with increasing vertical displacement and then leveling-off. The leveling-off values are much larger than those for the MRN data as one would expect due to the increased altitude. In this data the leveling-off value is about $3500 \text{ m}^2/\text{sec}^2$ corresponding to $\sigma \approx 42 \text{ m/sec}$, in reasonable agreement with Figure 7 for this height range.

Figure 15 shows the vertical structure functions for the vertical winds. The raw vertical wind data were used in the computations with no daily differencing. However, since essentially all of the vertical wind should be the irregular component this is considered appropriate. Both functions, for data below and above 110 km, show a linear log-log increase over small vertical displacements with slopes of 1.32 and 1.52 respectively. The function for the data above 110 km does not have a definite leveling-off point, whereas, the function for the data below 110 km levels off at a value of $250 \text{ m}^2/\text{sec}^2$ corresponding to $\sigma \approx 11 \text{ m/sec}$. This σ is much smaller than the above calculated σ -value for the horizontal winds in the same altitude range. Again, this is as expected because the vertical amplitudes of atmospheric gravity wave motions are expected to be smaller than the corresponding horizontal amplitudes.

The ROBIN daily difference data and ROBIN irregular wind data from harmonic analysis were analyzed similarly and the results are shown in Table 6. The results of the ROBIN data were not averaged with the results of the MRN data because the resultant values were significantly different. It is suspected that something peculiar is occurring in the ROBIN data and consequently, the ROBIN

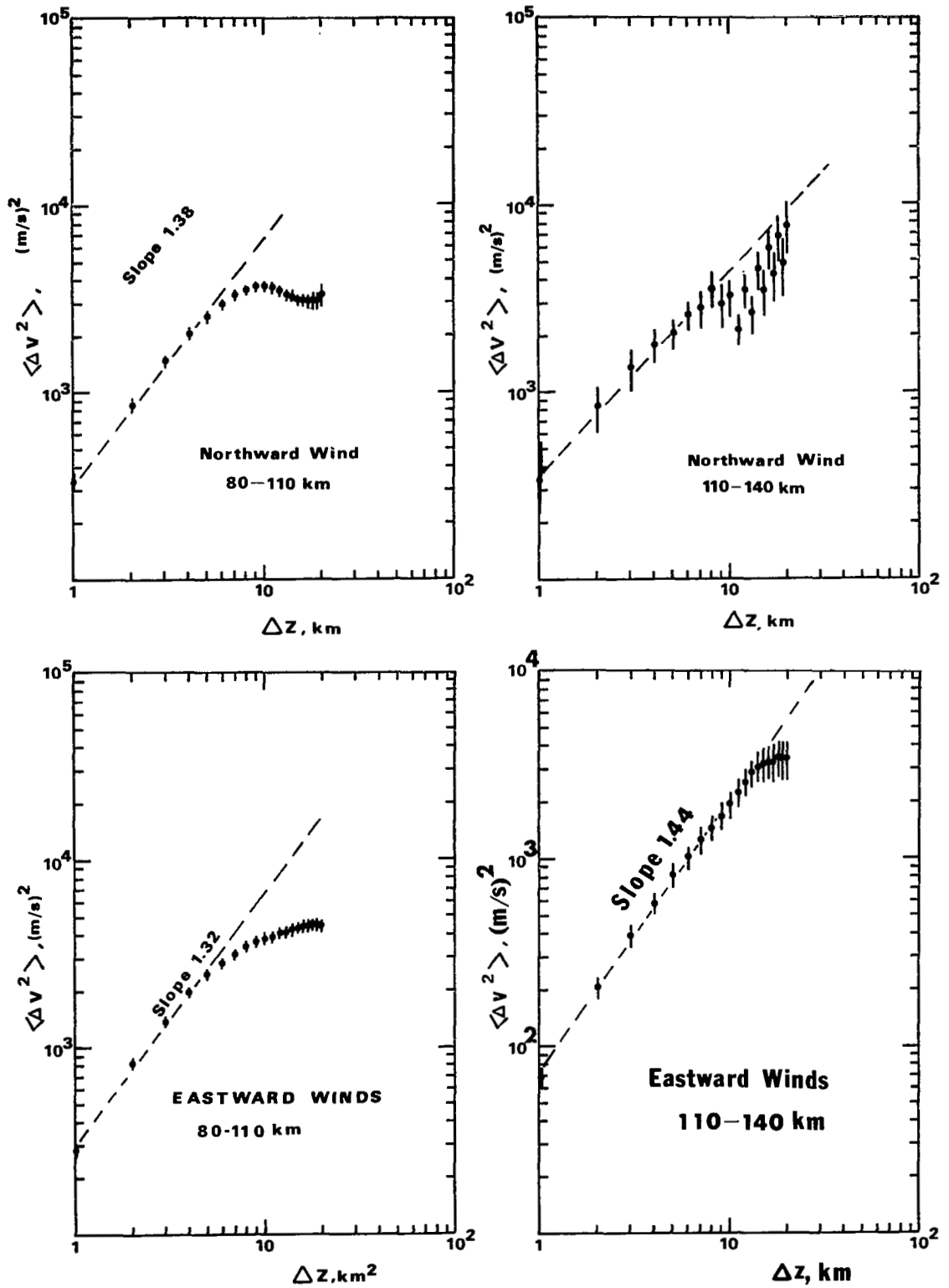


Figure 14. Vertical structure functions of chemical release and grenade release horizontal wind data determined by the daily difference method.

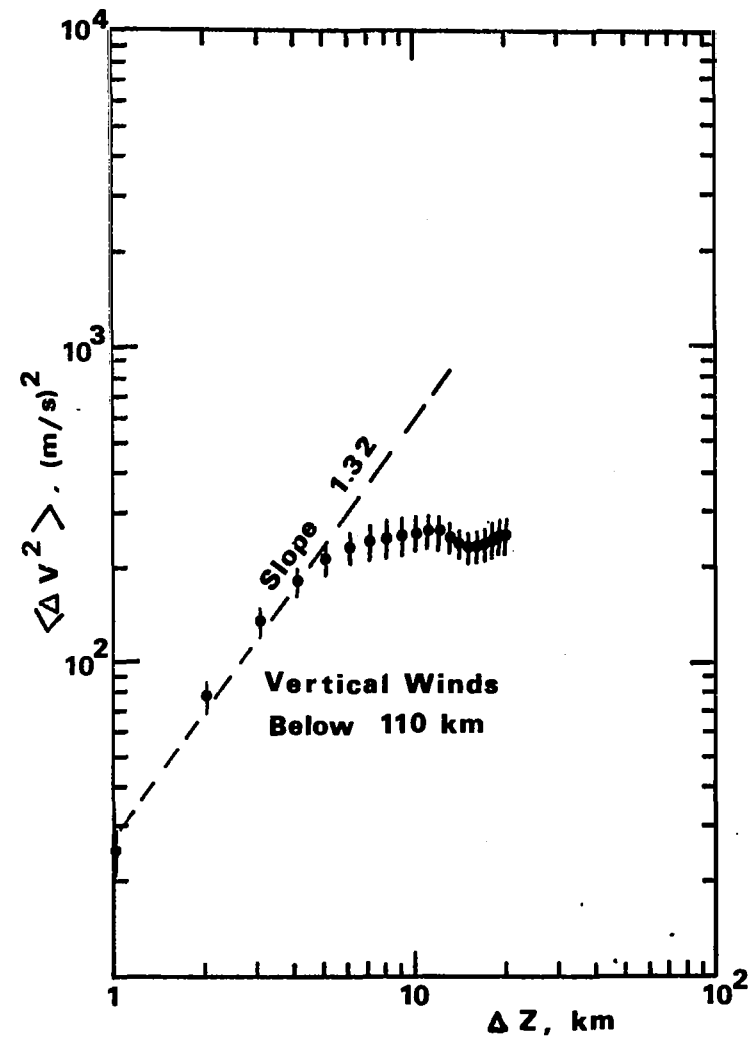
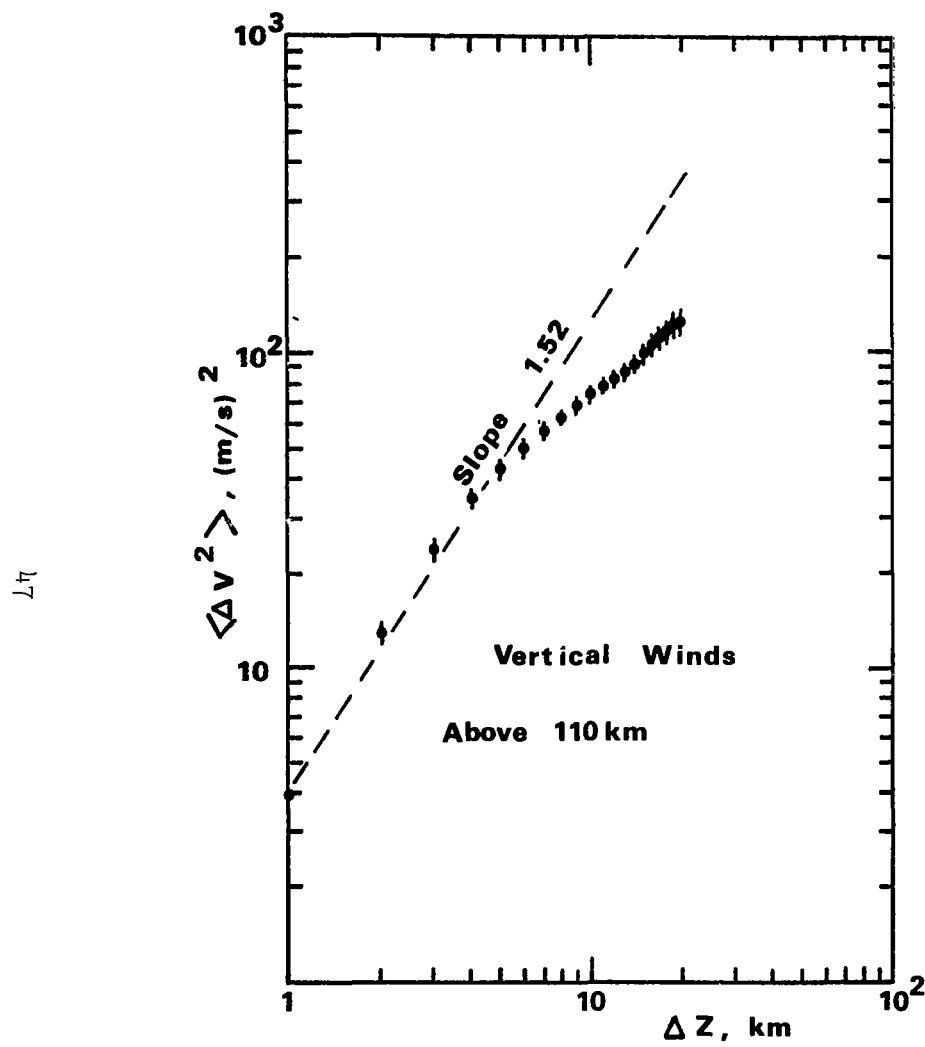


Figure 15. Vertical structure of chemical release vertical wind data.

values were kept separate.

Table 6 also gives a summary of the results of the vertical structure function analysis and other results.

Justus⁽⁴⁴⁾ analyzed chemical release data from Yuma to obtain a vertical structure function via an analysis method which is different from the method used in this report. His results are shown in Figure 16 and they agree with the results summarized in Table 6, but the exponent $n = 1.6$ is slightly larger. If the exponent values n of Table 6 are interpreted via equation (12) as resulting from a continuous power law spectrum, then spectra of the vertical wave number k would follow a power law $\phi(k) \propto k^{-(1+n)}$. The tendency of the Table 6 values of n to increase with altitude would thus indicate a changing spectrum with height.

The dominant vertical scale of the irregular motion can also be observed from the vertical structure functions. The half wavelength of the dominant vertical scale is given as the minimum height displacement for which the vertical structure function begins to level off. An average value for the dominant vertical scale of the MRN data (data heights from 45 to 65 km) is about 7 or 8 km. The same average value was found also for the chemical release data which is at a height of around 110 km. These results are in agreement with theoretical predictions by Tchen⁽²⁷⁾, who stated that the minimum vertical scale of internal gravity waves should be proportional to the pressure scale height. The scale height for the height regions of concern is fairly constant at about 8 km. Earlier experimental support of the correlation between scale height and minimum vertical scale was given by Justus⁽⁷⁵⁾ in his analysis of chemical release data. However, the structure function scale of 7 km at the 45 to 65 km level

TABLE 6. SUMMARY OF STRUCTURE FUNCTION INITIAL
EXPONENTS n AND MAGNITUDES σ INFERRED FROM LEVELING-OFF VALUES

Data	Height Range (km)	V_{ns}		V_{ew}		Temperature			Pressure			Density			V_z (m/sec)
		n	σ (m/sec)	n	σ (m/sec)	n	σ	n	n	n	n	n	n		
MRN	45-65	1.06	10	0.94	11	1.09	1.6	0.82	0.65						
ROBIN (Daily Diff.)	45-65	0.69	18	0.60	18	0.56	--	1.32	0.72						
ROBIN (Harmonic Analysis)	45-65	0.84	--	0.68	--	1.52	6	1.48	1.40						
Chemical Release	80-110	1.32	42	1.32	47					1.32	11				
Chemical Release	110-140	1.08	--	1.44	42					1.52	--				

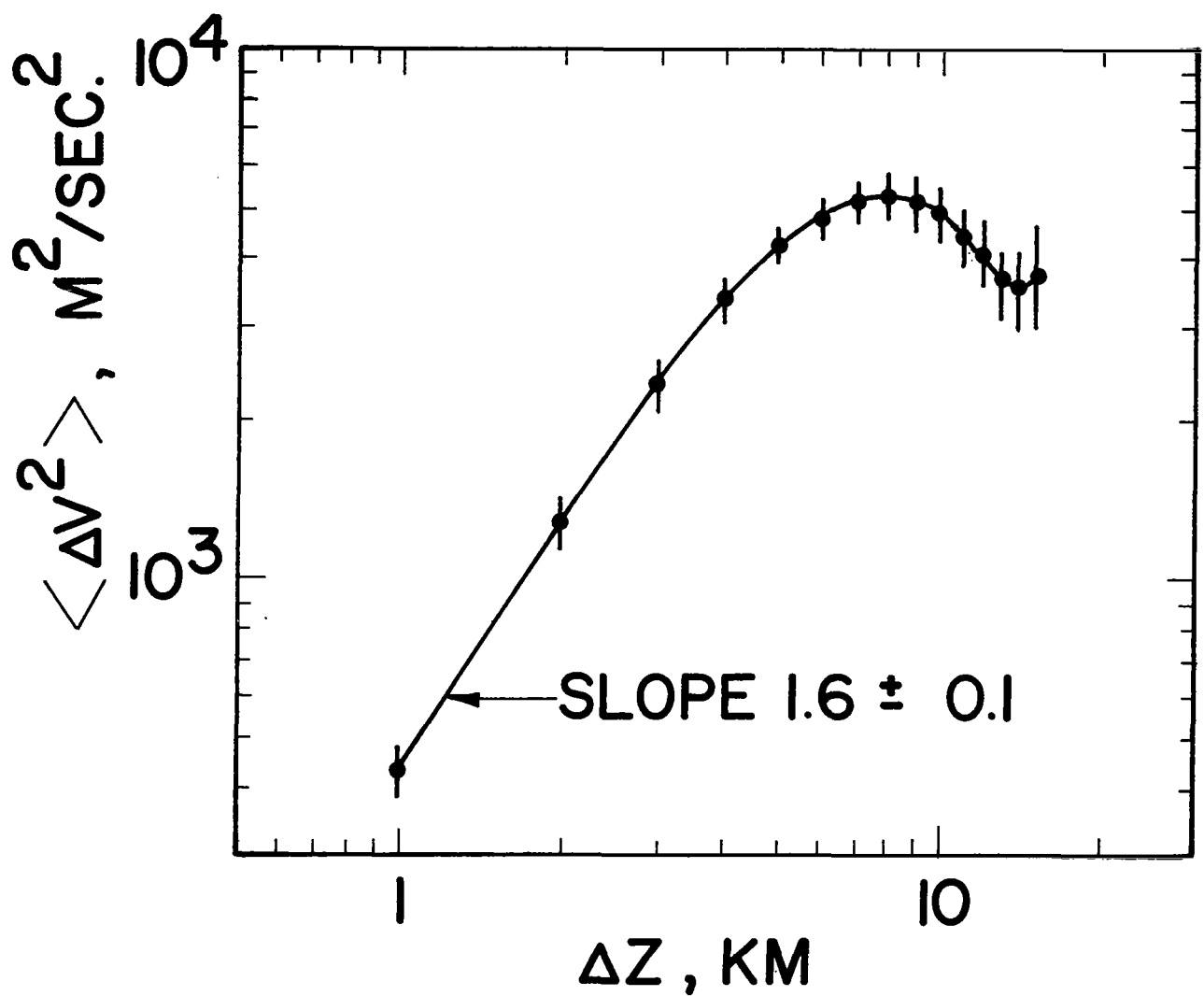


Figure 16. Vertical structure function of chemical release data previously analyzed by Justus⁽⁴⁴⁾ using a deviation-from-the-mean technique.

is contrary to the estimates by Webb⁽⁷⁶⁾ and others of a vertical scale of about 2 km in that height range. These lower estimates have come from subjective estimates of layer thickness in the wind profiles or correlation scales of deviations from 5 km vertical means. The first of these may be deficient because of tendency for the eye to ignore larger scale undulations for the smaller scale "wiggles" in the profile, and the second method a priori excludes the computation of a scale larger than 5 km.

5. HORIZONTAL STRUCTURE FUNCTION DATA.

The horizontal structure function is defined as

$$D(r) = \langle [V(x) - V(x + r)]^2 \rangle \quad (32)$$

where V may be the horizontal velocity (made up of the two horizontal velocity components), the pressure, temperature, or density; x is the horizontal coordinate vector; and r is the horizontal displacement vector. The structure function depends only on r , the magnitude of the vector r .

Data. The horizontal structure function of the irregular winds can be estimated by taking differences in winds determined from up and down leg trails or by taking differences in winds determined from two simultaneous measurements separated by a small horizontal distance. The horizontal separation of the measurements provides the horizontal displacement in the structure function computation. Data meeting these qualifications were found in the chemical release data obtained from rockets fired at Eglin AFB, Florida⁽⁵⁰⁾ and in the chemical release data obtained from the gun firings at Barbados, West Indies, and Yuma, Arizona^(51,77). The altitude range of these data is about 80 to 140 km.

In the lower altitudes, an attempt was made to use the ROBIN data⁽⁵³⁾, but there were not enough data available to obtain statistically meaningful information. Also, the same was true for pressure, temperature and density data. Although some data were available^(78,79), there were not enough data to determine any trends of the horizontal structure function for these quantities. However, the results computed here and averaged with structure function values reconstructed from correlation values reported by Mahoney and Boer⁽⁸⁰⁾, Cole and Kantor⁽⁸¹⁾, and Lettau⁽⁸²⁾ did produce reasonable results.

Analysis. Figure 17 shows the horizontal structure function of the horizontal winds. Horizontal structure function data for the vertical winds was also obtained from the chemical release data and is shown in Figure 18. Each data point on these figures represents the average of several data points which were grouped according to small horizontal separation intervals. The data point at the largest separation (450 km) represents the results of differing one pair of chemical release wind profiles reported by Blamont⁽⁸³⁾. The line through the data points of Figure 17 represents variation according to the power law

$$D(r) = \text{const. } (r)^{2/3} \quad (33)$$

and is seen to be in reasonable agreement with the observed data. This is also in agreement with previous results reported by Justus and co-workers^(16,77). Such a power law would correspond to a spectrum of horizontal wave numbers k of the form $\phi(k) \propto k^{-5/3}$. One of the theoretical results of two dimensional turbulence⁽⁸⁴⁾ is that a -5/3 spectrum would lead to an energy cascade up the spectrum to higher scales. Therefore it may be that the gravity wave field in the upper atmosphere, in addition to losing energy by damping and the generation of turbulence, may also serve as a partial energy source for larger scale motions, e.g. planetary waves and synoptic scale variations. The results of Figure 17 are compatible with a magnitude (σ) of about 40 m/s and a horizontal scale (half wave length) on the order of 500 km.

Conclusions from the vertical winds structure function in Figure 18 are less certain. One interpretation as shown would yield a power law of 1.06 at small scales and indicate a horizontal scale of about 20 - 30 km. The fact that the horizontal scale of the vertical winds is so much smaller than the

$\eta \zeta$

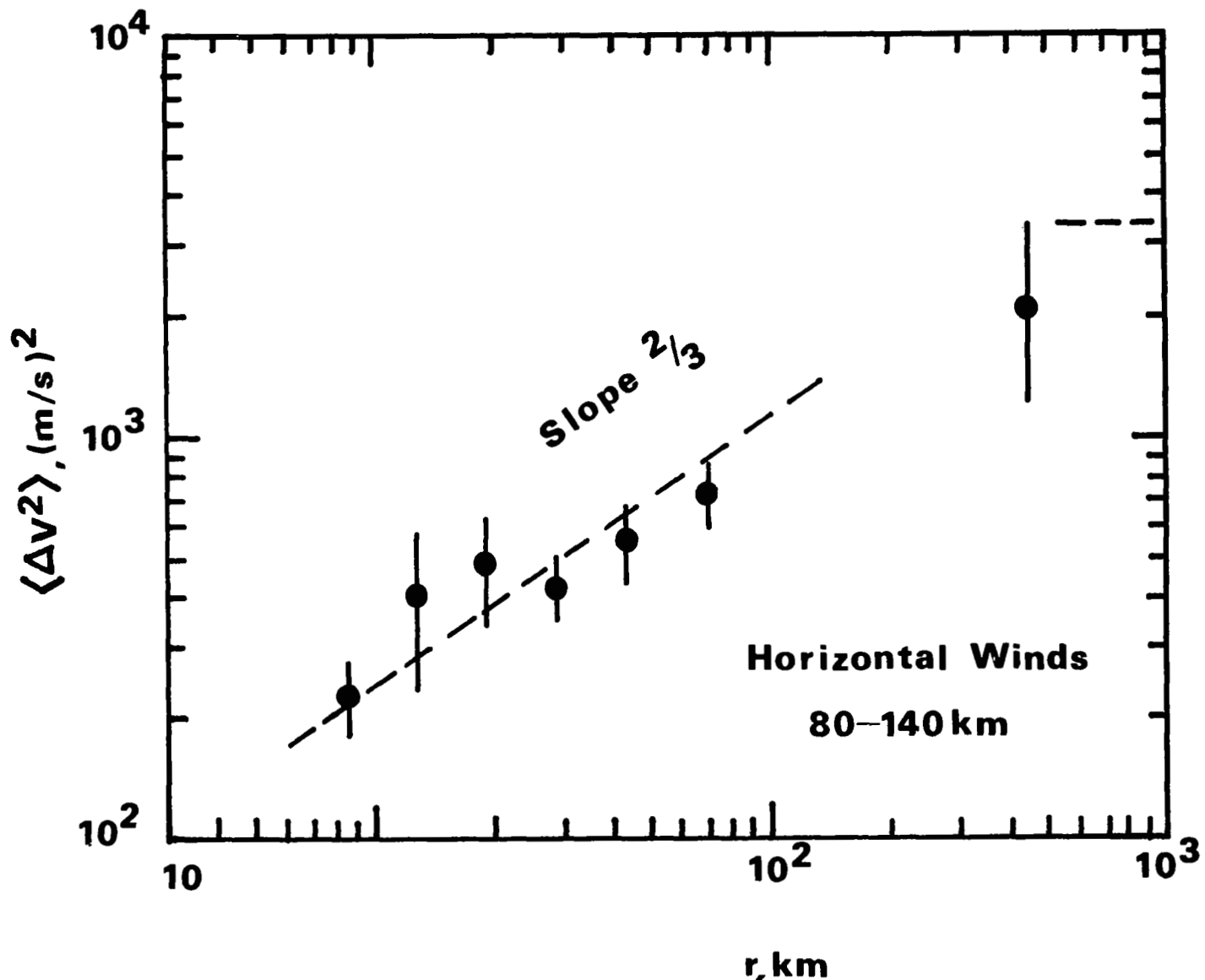


Figure 17 Horizontal structure function of the horizontal chemical release winds.

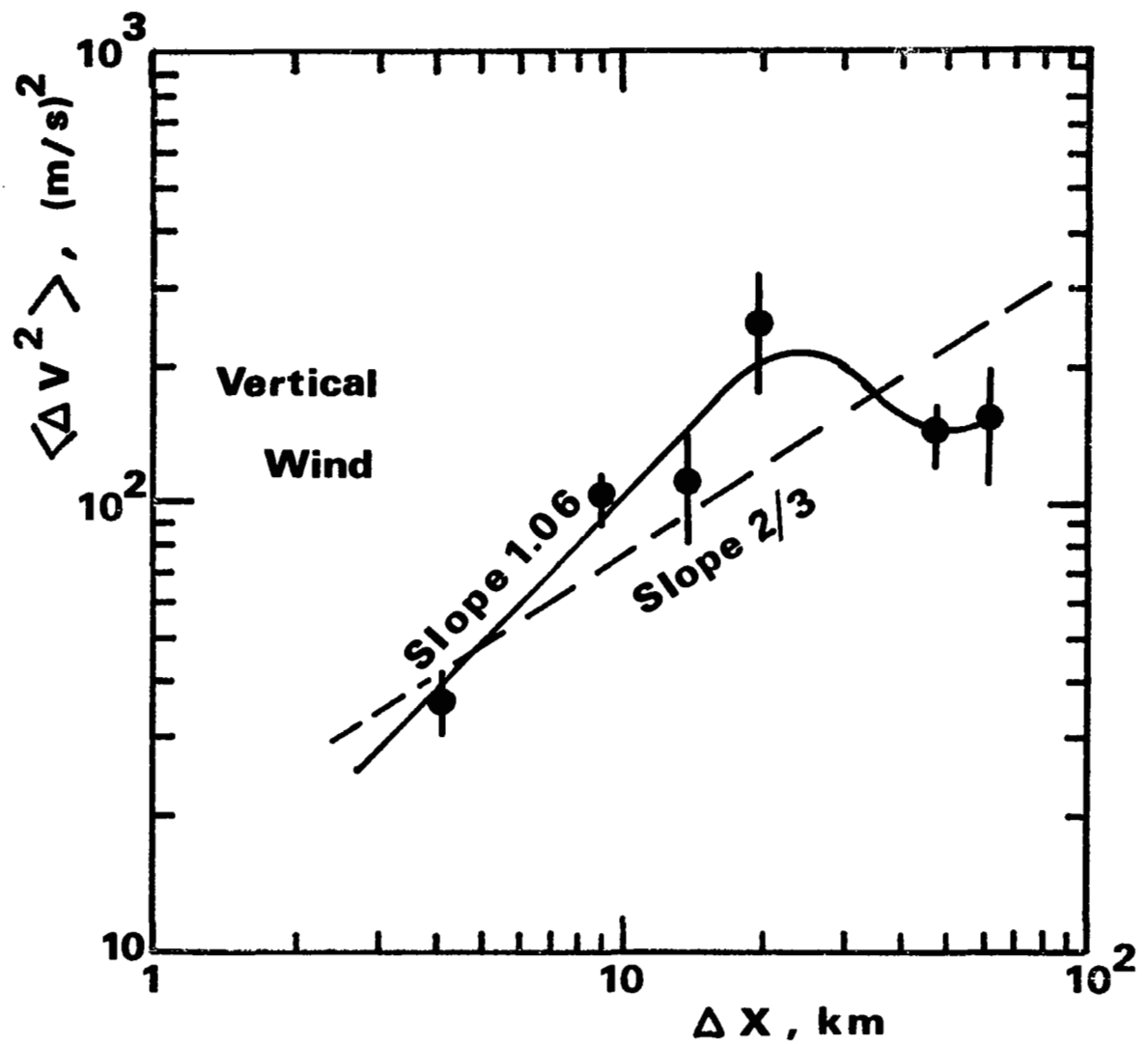


Figure 18. Horizontal structure function of the vertical chemical release wind.

scale for the horizontal winds indicates that the small scale waves have larger contributions from vertical components than do the large scale waves.

The horizontal structure function of the horizontal winds in the 45 - 65 km range are shown in Figure 19. The three data points at the largest scales are from Cole and Kantor⁽⁸¹⁾ and other data points were averaged from the other available data. The 2/3 power law fits the data reasonably well at small scales and the structure function at larger scales indicates a horizontal scale of about 100 km and a magnitude of about 10 m/s, somewhat lower than inferred earlier in this report.

57

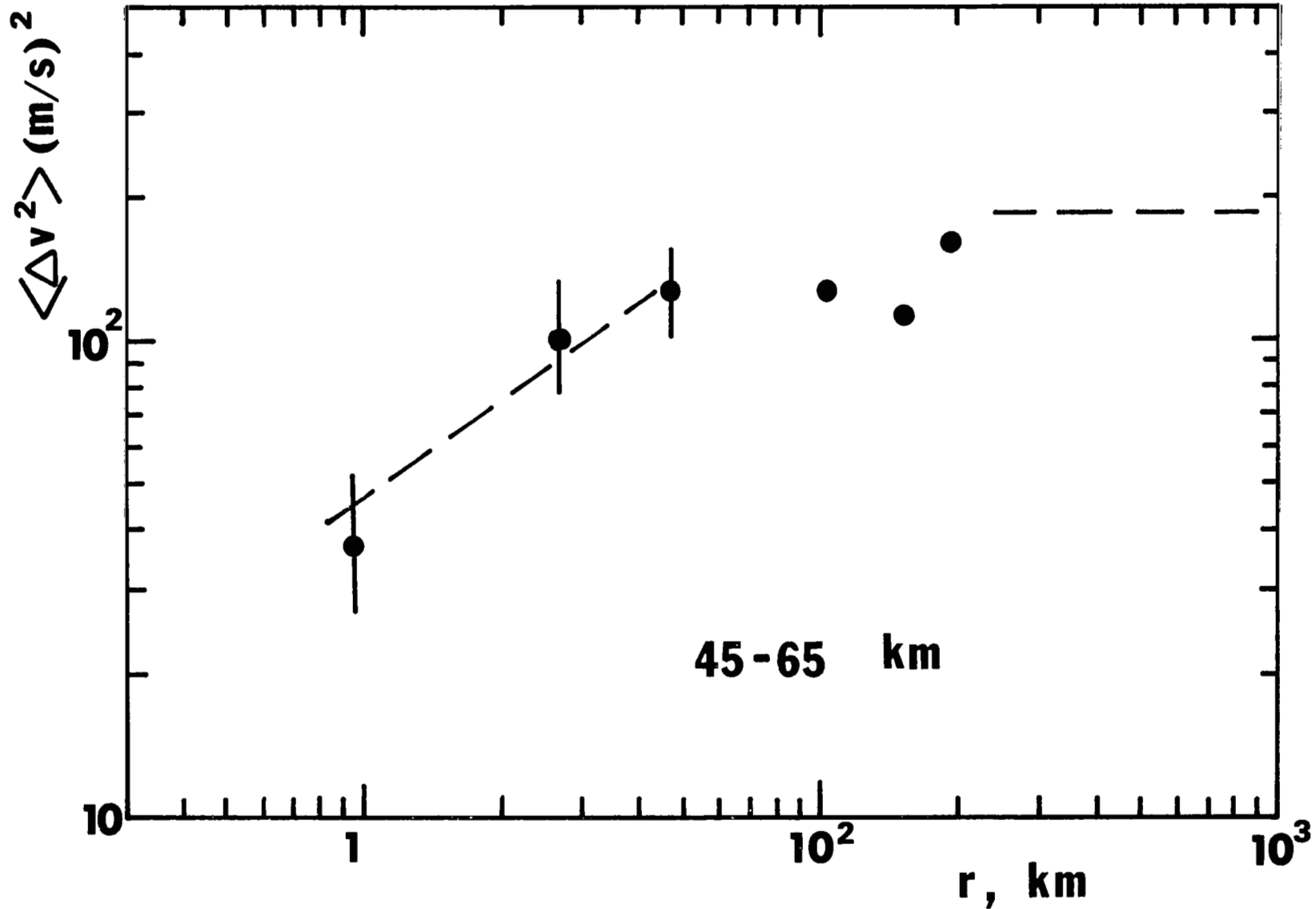


Figure 19. Horizontal structure function of the ROBIN data horizontal winds.

6. TIME STRUCTURE FUNCTION DATA

The time structure function is defined as

$$D(\Delta t) = \langle [V(t) - V(t + \Delta t)]^2 \rangle \quad (34)$$

where V may be a velocity component, pressure, temperature, or density, t is the time and Δt is the time separation.

Data. Profiles of irregular winds, pressure, temperature and density were obtained by subtracting tidal contributions from raw data. The tidal contributions were found by performing a harmonic analysis on a data set for the diurnal and semidiurnal cycles as explained earlier (see equation (20)). Sufficient data for 9 different data sets were found from MRN data. The results of the harmonic analysis compared very well with previous work that had been performed on essentially the same data⁽⁸⁵⁻⁹⁰⁾.

After the tidal contributions had been extracted from a data set, the remaining data gave a series of irregular winds profiles as a function of time. The time intervals between the irregular data profiles provides the time separation needed for the calculation of the time structure function.

Analysis. The calculated time structure functions for the northward and eastward velocity components are shown in Figure 20. Both functions show a definite oscillatory motion which indicates the existence of significant motion with dominant periods. The dominant time scale (half period) is about 2 - 3 hours. However, the oscillatory motion is centered on a value which is sufficiently high to indicate that there exists also irregular motion with a continuous distribution of periods. The lines drawn in the figure have slopes of 1.07 for the northward winds and 1.63 for the eastward winds. However these

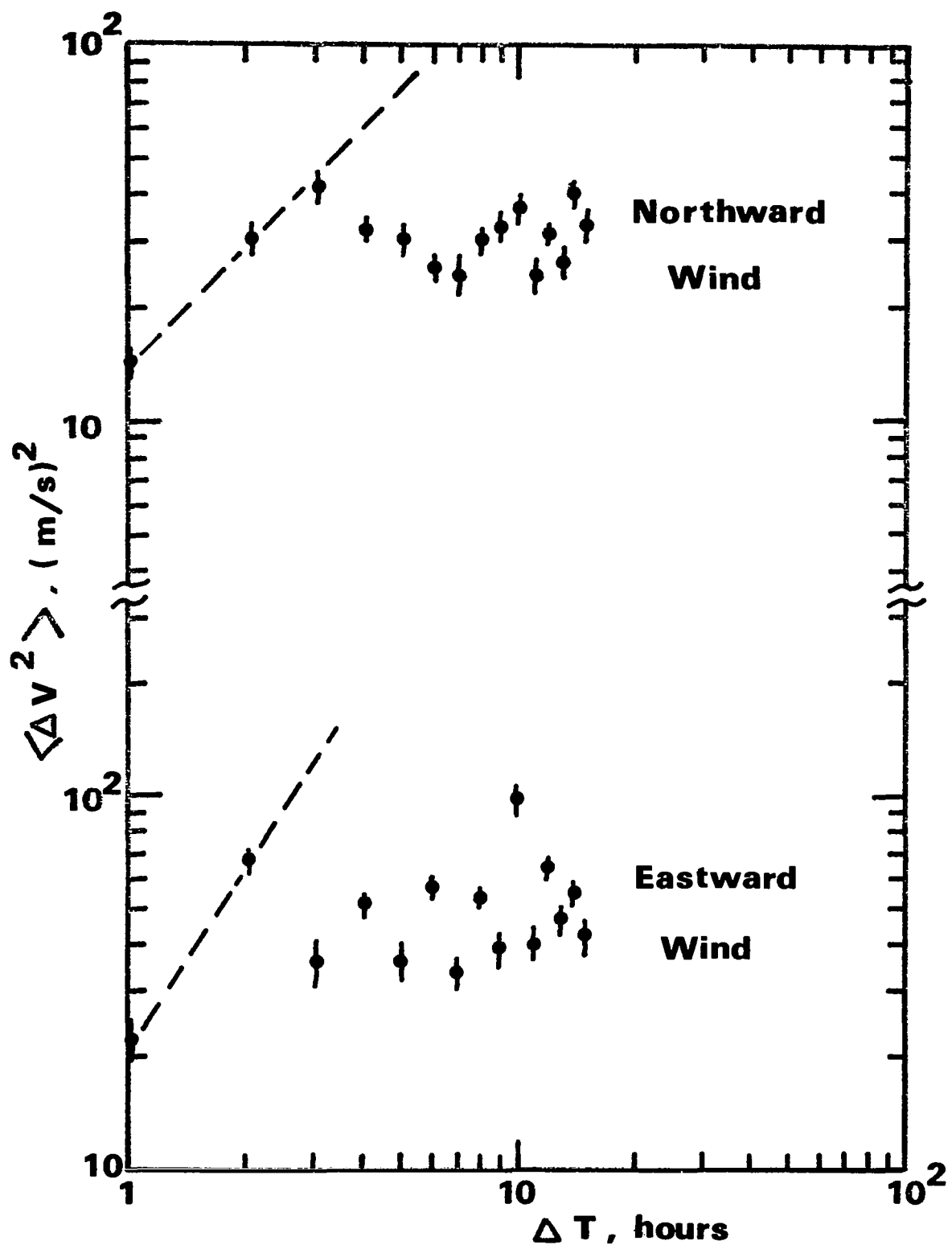


Figure 20. Average time structure function of MRN and ROBIN data horizontal winds in the 45 - 65 km height range.

values are highly uncertain due to the lack of data at short time displacements.

A time structure function shown in Figure 21 was constructed from the correlation data of Greenhow and Neufeld⁽⁹¹⁾. This was done by using equation (9) and taking the rms irregular velocity to be 25 m/s, the value reported by Greenhow and Neufeld. These results have a power law behavior at small time displacements with a 2/3 power of Δt . This result appears to contradict the MRN results but is in agreement with the horizontal structure functions since an application of Taylor's hypothesis would say that time structure functions and horizontal structure functions should behave similarly. The data of Figure 21 indicates a dominant time scale of about 3 hours, slightly higher than the MRN data, but the lengthening of the time scale is to be expected at the higher altitudes.

Justus⁽⁴⁴⁾ has calculated the time structure function of irregular winds for the altitude range near 100 km. His results are given in Figure 22. At this higher altitude there seems to be less contribution from a single strongly dominant period in the irregular motions and more of a continuous distribution of periods. The slope of the linear increase is 1.5 which tends to confirm the higher of the slopes found at the lower altitude. The time scale at the higher altitudes is significantly increased and is of the order of 10 hours.

T9

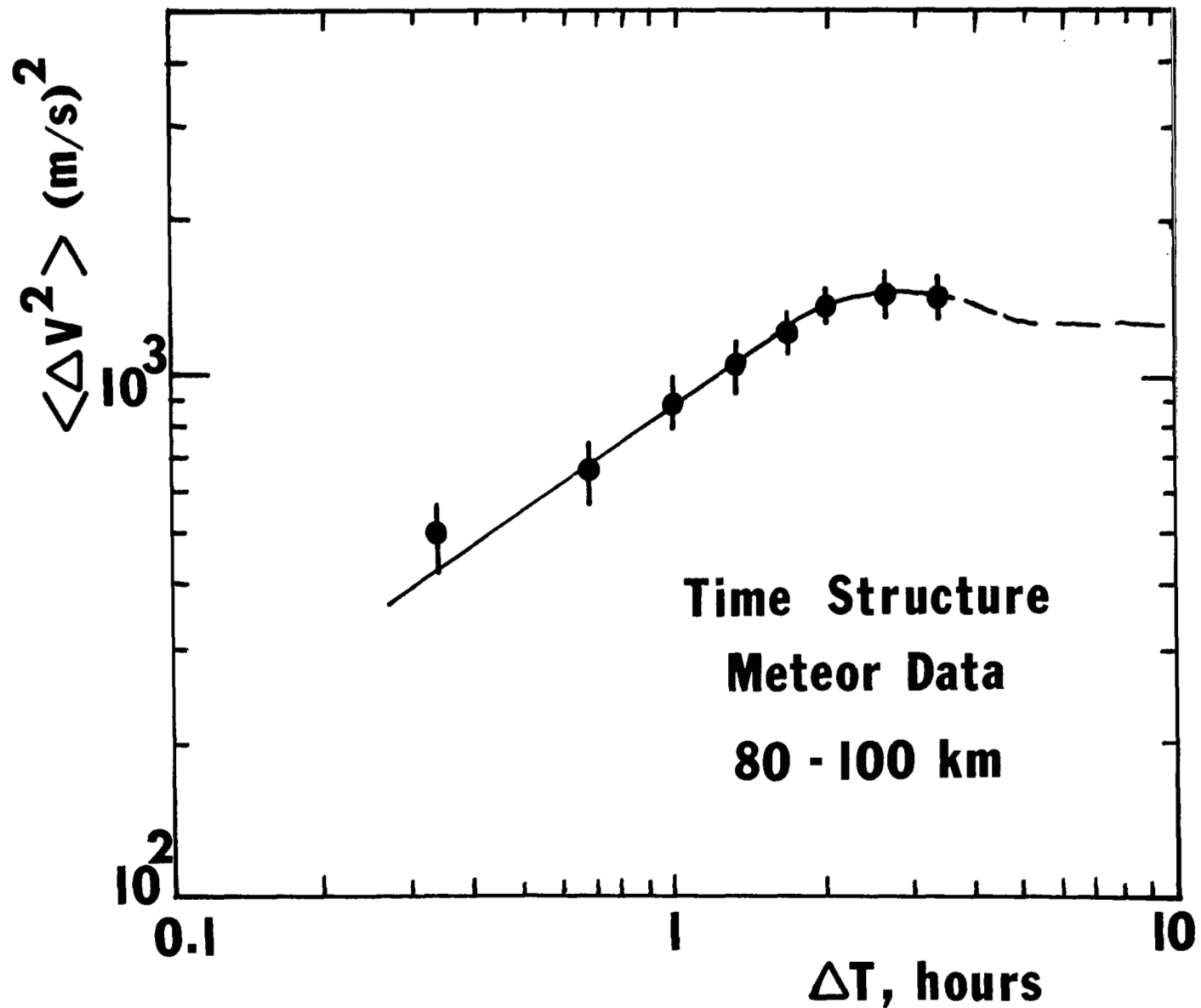


Figure 21. Time structure function of Greenhow and Neufeld meteor winds⁽⁹¹⁾ reconstructed from their correlation curve.

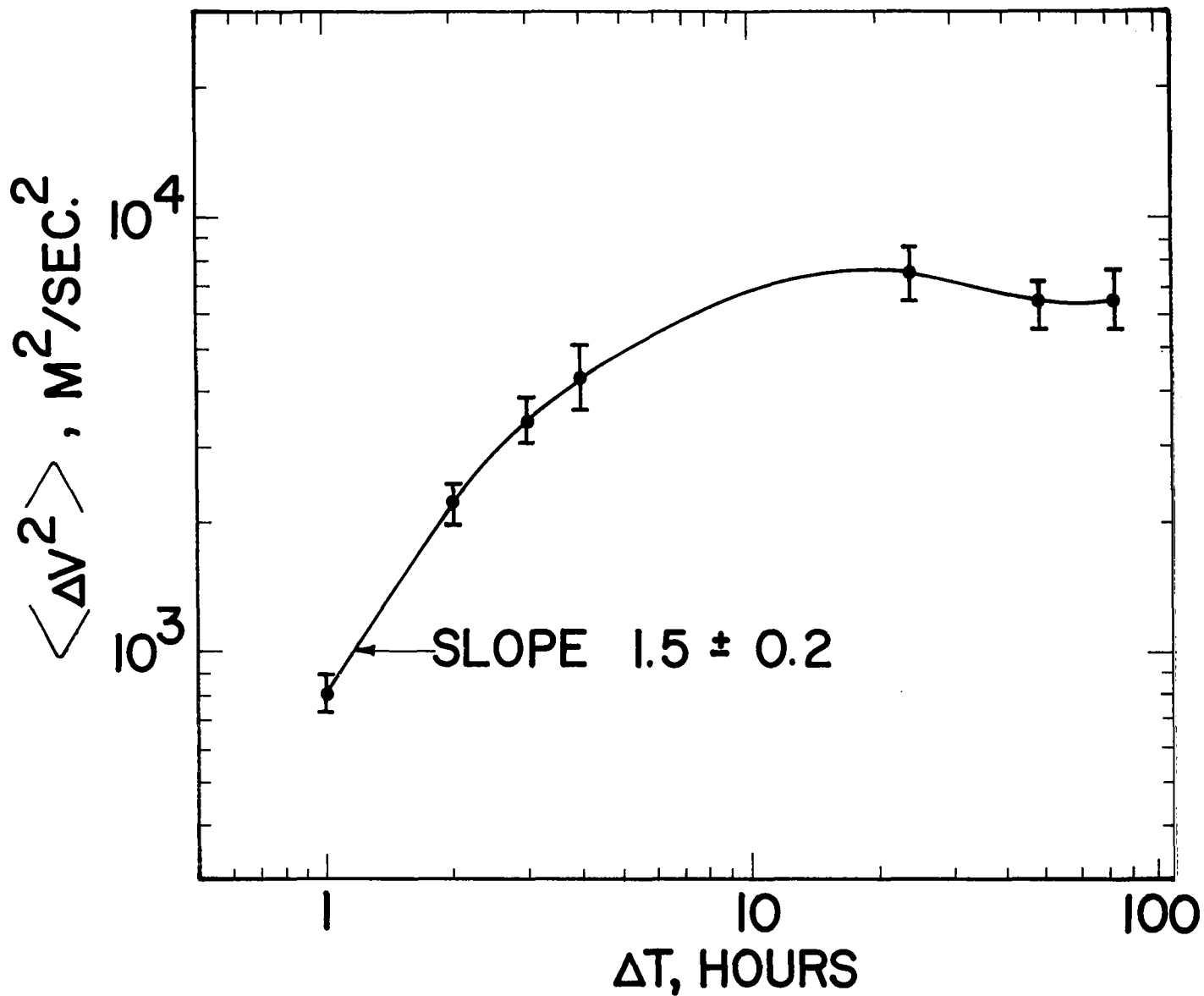


Figure 22. Time structure of chemical release horizontal winds previously analyzed by Justus⁽⁴⁴⁾ using a deviation-from-the-mean technique.

7. THE EFFECTIVE FREQUENCY SPECTRUM ENCOUNTERED BY A SPACECRAFT

The analysis of the structure functions presented in the previous sections indicate that the irregular wind, pressure, density, and temperature fields in the 50 - 200 km region can be considered as a more-or-less continuous spectrum, except that in certain cases, such as the vertical wave number spectrum in the 45 - 65 km region, single modes of specific wavelength must be added to the otherwise continuous spectrum. This leads to the conclusion that the effects of the gravity wave field on spacecraft traversing these altitude regions can be analyzed in terms of the spectral techniques of turbulence. However, the results show that significant anisotropy exists in that the horizontal scales are significantly larger than vertical scales. In view of the nearly isotropic conditions in the horizontal, analysis in terms of axisymmetric spectra is suggested, with the axis of symmetry being in the vertical.

The coordinates of the analysis are indicated in Figure 23. The x, y, z system has x and y axes in the horizontal plane and z in the vertical direction. The x direction has been conveniently chosen to be along the azimuth of the spacecraft trajectory. The elevation of the spacecraft trajectory is the angle θ and the x', y', z' axes are those which are rotated through this angle θ . Thus x' is along the direction of flight of the spacecraft. The displacement r along the x' axis is the distance of travel of the spacecraft in an arbitrary time interval τ . With the speed of the spacecraft given by U , then r and τ are related by $r = Ut$. The displacement r can be broken into component displacements r_1 and r_3 in the horizontal and vertical directions.

Frequency Spectrum of Scalars. The frequency spectrum $\phi(\omega)$ of a scalar property, say temperature T' , is related to the time correlation $R(\tau)$ by the

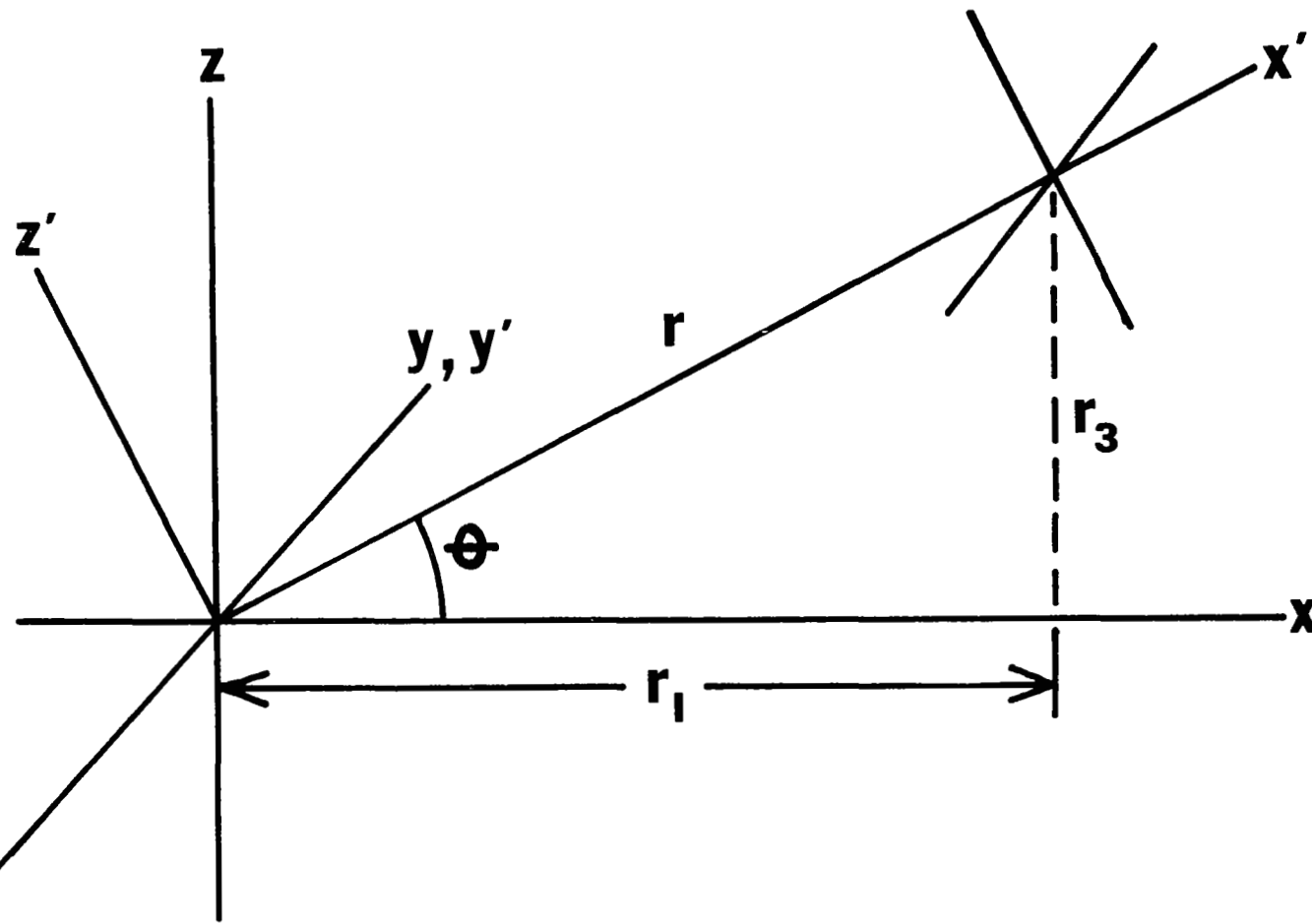


Figure 23. Coordinate systems used in the analysis of observed frequency spectra on spacecraft in a trajectory elevated at an angle θ .

spectral transform relation

$$\theta(\omega) = \frac{\langle T'^2 \rangle}{\pi} \int_0^\infty \cos \omega \tau R(\tau) d\tau \quad (35)$$

The problem thus is to determine what the correlation $R(\tau)$ is from such measurable quantities as those presented in previous sections of this report. The assumption is made that the spacecraft speed U is sufficiently large that Taylor's hypothesis can be used so that $R(\tau)$ is the same as $R(r)$ where $r = Ut$. It is further assumed that the correlation $R(r)$ is the product of correlations which depend only on the components of r , i.e.

$$R(r) = \rho_1(r_1) \rho_3(r_3) \quad (36)$$

If the horizontal and vertical structure functions $D_1(r_1)$ and $D_3(r_3)$ have been determined instead of correlations, then, from equation (9), equation (36) can be written as

$$R(r) = (1 - D_1(r_1)/2 \langle T'^2 \rangle)(1 - D_3(r_3)/2 \langle T'^2 \rangle) \quad (37)$$

where r_1 and r_3 are given by

$$\begin{aligned} r_1 &= U \cos \theta \tau \\ r_3 &= U \sin \theta \tau \end{aligned} \quad (38)$$

Thus any particular measured or model form for structure functions in (37) or correlation functions in (36) can be substituted into (35). The effective frequency spectrum would, because of equation (38), depend on the spacecraft velocity U and the elevation angle of the trajectory θ . It is beyond the scope of this report to evaluate actual frequency spectra. However, the results of the previous sections indicate that a reasonable model would be given

by

$$R(r) = [1 - (r_1/r_{10})^m][1 - (r_3/r_{30})^n] \quad (39)$$

if $r_1 < r_{10}$ and $r_3 < r_{30}$ or $R(r) = 0$ otherwise, where r_{10} and r_{30} are respectively horizontal and vertical structure function scales and m and n are respectively the power law exponents of the horizontal and vertical structure functions at small scales.

Frequency Spectrum of Velocity. Considerable additional complication is introduced when spectra of vector quantities, such as velocity, are considered. Not only must we consider longitudinal and transverse correlations but transformations between the horizontal - vertical system of coordinates (x, y, z) and the trajectory system of coordinates (x', y', z'). The spectrum of transverse (y') velocity u_2 is the same in either system of coordinates

$$\phi_{22}'(\omega) = \frac{\langle u_2^2 \rangle}{\pi} \int_0^\infty \cos \omega \tau R_{22}'(\tau) d\tau \quad (40)$$

and the correlation function is likewise equal in both coordinates $R_{22}'(\tau) = R_{22}(\tau)$. But the "vertical" (z') velocity spectrum in the trajectory system must be transformed since we have

$$\phi_{33}'(\omega) = \frac{\langle u_3^2 \rangle}{\pi} \int_0^\infty \cos \omega \tau R_{33}'(\tau) d\tau \quad (41)$$

and as can be easily shown from the properties of coordinate rotation

$$\begin{aligned} R_{33}'(\tau) &= \cos^2 \theta R_{33}(\tau) + \sin^2 \theta R_{11}(\tau) \\ &\quad - \sin \theta \cos \theta [R_{13}(\tau) + R_{31}(\tau)] \end{aligned} \quad (42)$$

The correlations may also be expressed as function of r_1 and r_3 given by equation

(38). However, the form of dependence required by the axisymmetric condition are somewhat more complicated than (36). The form of the normalized correlation tensor $R_{ij}(r)$ in an axisymmetric field is given by⁽⁹²⁾

$$R_{ij}(r) = A r_i r_j + B \delta_{i3} \delta_{j3} + C \delta_{ij} \\ + D(r_i \delta_{j3} - r_j \delta_{i3}) \quad (43)$$

where the axis of symmetry has been specified as the vertical, and the coefficient functions A, B, C, and D are functions of the magnitude r and the vertical component magnitude $|r_3|$. Of particular interest are the following specific terms of (43)

$$R_{11}(r) = A r_1^2 + C \\ R_{22}(r) = A r_2^2 + C \\ R_{33}(r) = A r_3^2 + B + C \\ R_{13}(r) + R_{31}(r) = 2A r_1 r_3 \quad (44)$$

If we now assume that $A = A_1(r_1) A_3(r_3)$, $B = B_1(r_1) B_3(r_3)$ etc. then the easily measured correlations (and those which can be related by equation (9) to the structure functions discussed in the previous sections) can be written as

$$R_H(r_1) = R_{11}(r_1) + R_{22}(r_1) = K_3 A_1 r_1^2 + 2C_1 \\ R_H(r_3) = R_{11}(r_3) + R_{22}(r_3) = 2C_3 \\ R_V(r_1) = R_{33}(r_1) = B_1 + C_1 \\ R_V(r_3) = R_{33}(r_3) = K_1 A_3 r_3^2 + B_3 + C_3 \quad (45)$$

Where $K_1 = A_1(0)$ and $K_3 = A_3(0)$

Thus A_1 , A_3 , B_1 , B_3 , C_1 , and C_3 are 6 unknowns required to determine the correlations and spectra completely, but the relations (45), with the correlations considered measured or otherwise known, constitute only 4 equations for these 6 unknowns.

However, if we also assume that, in analogy with (36), the relations

$$\begin{aligned} R_H(r) &= R_H(r_1) R_H(r_3)/2 \\ R_V(r) &= R_V(r_1) R_V(r_3) \end{aligned} \quad (46)$$

(the denominator of 2 in the horizontal correlation is required to maintain the proper normalization $R_H(0) = 2$) then it can be shown (see the Appendix) that

$$\begin{aligned} A_1(r_1) &= K_1 R_V(r_1) \\ A_3(r_3) &= K_3 R_H(r_3)/2 \\ B_1 &= B_3 = 0 \\ C_1(r_1) &= R_V(r_1) \\ C_3(r_3) &= R_H(r_3)/2 \end{aligned} \quad (47)$$

where the constants K_1 and K_3 and microscales of the correlations (defined in the Appendix) must satisfy the relations

$$\begin{aligned} K_1 K_3 &= (2/\lambda_{V1}^2 - 1/\lambda_{H1}^2)/2 = \\ &(1/\lambda_{H3}^2 - 2/\lambda_{V3}^2)/8 \end{aligned} \quad (48)$$

Thus the correlation $R_{22} = R_{22}'$ which is to be employed in (40) for the determination of the y' velocity spectrum is given by

$$R_{22}(\tau) = R_V(U \cos \theta \cdot \tau) R_H(U \sin \theta \cdot \tau)/2 \quad (49)$$

and the correlations to be employed in (42) and (41) for the determination of the z' velocity spectrum are given by

$$\begin{aligned} R_{11}(\tau) &= (K_1 K_3 r_1^2 + 1) R_V(r_1) R_H(r_3)/2 \\ R_{33}(\tau) &= (K_1 K_3 r_3^2 + 1) R_V(r_1) R_H(r_3)/2 \\ R_{13}(\tau) + R_{31}(\tau) &= K_1 K_3 R_V(r_1) R_H(r_3) r_1 r_3 \end{aligned} \quad (50)$$

where r_1 and r_3 are given by (38).

Thus any particular measured or model form of the correlation functions $R_V(r_1)$, $R_H(r_3)$, $R_V(r_3)$, and $R_H(r_1)$ which are consistent in form with the equation (48) can be used in the above equations and substituted into (40) and (41) to determine the desired velocity spectra. The effective frequency spectra are, because of equation (38), dependent on the spacecraft velocity U and elevation angle of trajectory θ . If horizontal and vertical structure functions have been determined instead of correlation functions, then from equation (9) the following relations can be employed instead:

$$\begin{aligned} R_H(r_1) &= 1 - D_H(r_1) / [2(\langle u^2 \rangle + \langle v^2 \rangle)] \\ R_H(r_3) &= 1 - D_H(r_3) / [2(\langle u^2 \rangle + \langle v^2 \rangle)] \\ R_V(r_1) &= 1 - D_V(r_1) / 2 \langle w^2 \rangle \\ R_V(r_3) &= 1 - D_V(r_3) / 2 \langle w^2 \rangle \end{aligned} \quad (51)$$

Again, it is beyond the scope of this report to evaluate actual frequency spectra. However, model correlations similar to equation (39) would be reasonable forms for the rough approximation of the measured results of the previous sections.

APPENDIX

Under the assumption of equation (46) the normalized correlations R_H and R_V become, after substitution from (45)

$$\begin{aligned} R_H(r) &= K_3 A_1 C_3 r_1^2 + 2C_1 C_3 \\ R_V(r) &= K_1 A_3 (B_1 + C_1) r_3^2 + B_1 B_3 + C_1 C_3 \\ &\quad + B_1 C_3 + C_1 B_3 \end{aligned} \quad (A1)$$

In order for these relations to be equivalent to the defining relations for R_H and R_V

$$\begin{aligned} R_H(r) &= A r_H^2 + 2C \\ R_V(r) &= A r_3^2 + B + C \end{aligned} \quad (A2)$$

where, because of the coordinates employed in Figure 23, $r_H = r_1$, then because we have assumed $A = A_1 A_3$, $B = B_1 B_3$, and $C = C_1 C_3$, the following relations apply between the coefficient function

$$\begin{aligned} A_3 &= K_3 C_3 \\ A_1 &= K_1 (B_1 + C_1) \\ B_1 C_3 + C_1 B_3 &= 0 \end{aligned} \quad (A3)$$

Since K_1 was defined as $A_1(0)$ and K_3 as $A_3(0)$ then (A3) shows that $C_3(0) = 1$ and $B_1(0) + C_1(0) = 1$. The normalization $R_H(0) = 2$ together with the value $C_3(0) = 1$ implies that $C_1(0) = 1$. Hence $B_1(0) = 0$. The last relation of (A3) may be written as

$$\frac{B_1(r_1)}{C_1(r_1)} = - \frac{B_3(r_3)}{C_3(r_3)} = \text{constant} \quad (\text{A4})$$

where the constancy is required by the fact that the first term depends only on r_1 and the second depends only on r_3 . Now since (A4) must hold for all values of r_1 then the value of the constant is $B_1(0) / C_1(0)$ which is zero. Thus

$$\begin{aligned} B_1(r_1) &= 0 \\ B_3(r_3) &= 0 \end{aligned} \quad (\text{A5})$$

for all values of r_1 and r_3 , and the first two relations of (A3) thus become

$$\begin{aligned} A_1(r_1) &= K_1 C_1(r_1) \\ A_3(r_3) &= K_3 C_3(r_3) \end{aligned} \quad (\text{A6})$$

and (45) simplifies to

$$R_H(r_1) = (K_1 K_3 r_1^2 + 2) C_1(r_1) \quad (\text{A7})$$

$$R_H(r_3) = 2 C_3(r_3) \quad (\text{A8})$$

$$R_V(r_1) = C_1(r_1) \quad (\text{A9})$$

$$R_V(r_3) = (K_1 K_3 r_3^2 + 1) C_3(r_3) \quad (\text{A10})$$

Relations (A5), (A6), (A8), and (A9) thus give the coefficient functions A_1 , A_3 , B_1 , B_3 , C_1 , and C_3 in terms of the correlations $R_H(r_3)$ and $R_V(r_1)$. Second order differentiation of the ratio of (A7) to (A9) and the ratio of (A10) to (A8) establish two equations which relate the constants K_1 and K_3 to the derivatives of the correlation functions. Since the resulting equations must be valid at all values of r_1 and r_3 then they can be evaluated by setting r_1 and r_3 to zero

and by noting that $R_V(0) = 1$, $R_H(0) = 2$, and all first order derivatives of R_H and R_V with respect to r_1 or r_3 at $r_1 = 0$ or $r_3 = 0$ are zero. The resulting equations are given by (42) where the second derivative terms evaluated at zero are defined in terms of microscales.

$$(d^2 R_H / dr_1^2) \Big|_{r_1 = 0} = -1/\lambda_{H1}^2$$

$$(d^2 R_H / dr_3^2) \Big|_{r_3 = 0} = -1/\lambda_{H3}^2$$

$$(d^2 R_V / dr_1^2) \Big|_{r_1 = 0} = -1/\lambda_{V1}^2$$

$$(d^2 R_V / dr_3^2) \Big|_{r_3 = 0} = -1/\lambda_{V3}^2$$

(A11)

REFERENCES

- (1) Hines, C. O., Can. J. Phys., 38, 1441 (1960).
- (2) Friedman, J. P., J. Geophys. Res., 71, 1033 (1966).
- (3) Pitteway, M. L. V., and C. O. Hines, Can. J. Phys., 41, 1935 (1963).
- (4) Hines, C. O., J. Atmos. Terr. Phys., 30, 845 (1968).
- (5) Hines, C. O., and C. A. Reddy, J. Geophys. Res., 72, 1015 (1967).
- (6) Hines, C. O., J. Atmos. Terr. Phys., 30, 837 (1968).
- (7) Hines, C. O., J. Atmos. Terr. Phys., 30, 851 (1968).
- (8) Hines, C. O., and W. H. Hooke, J. Geophys. Res., 75, 2563 (1970).
- (9) Cole, A. E., and A. J. Kantor, Proc. 3rd Nat'l. Conf. on Aerospace Meteorology, New Orleans, 465-471 (1968).
- (10) Mahoney, J. R., Proc. 3rd Aeronomy Conf. Univ. of Illinois Aeronomy Report No. 32, 125-132 (1969).
- (11) Theon, J. S., et al., J. Atmos. Sci., 24, 428 (1967).
- (12) Witt, G., Tellus, 14, 1 (1962).
- (13) Hines, C. O., A Jet Stream Source of Waves in Noctilucent Clouds, presented at the Symposium on Acoustic-Gravity Waves in the Atmosphere, Boulder, Colo., July (1968).
- (14) Haurwitz, B., and B. Fogle, Deep Sea Res., 16 (Suppl.), 85 (1969).
- (15) Greenhow, J. S., and E. L. Neufeld, Quart. J. Roy. Met. Soc., 87, 472 (1961).
- (16) Justus, C. G., and R. G. Roper, Meteor. Monographs, 9 (31), 122 (1968).
- (17) Spizzichino, A., And I. Revah, Space Research, 8, 679 (1967).
- (18) Kochanski, A., J. Geophys. Res., 69, 3651 (1964).
- (19) Knudsen, W. C., and G. W. Sharp, J. Geophys. Res., 70, 143 (1965).
- (20) Harris, K. K., et al., J. Geophys. Res., 74, 197 (1969).
- (21) Vasseur, G., and P. Waldteufel, J. Atmos. Terr. Phys., 31, 885L (1969).
- (22) Georges, T. M., ESSA Rept. IER 57-ITSA54, "Ionospheric Effects of Atmospheric Waves" (1967).

(23) Georges, T. M., ed. Symposium on Acoustic-Gravity Waves in the Atmosphere, Boulder, Colo., July (1968).

(24) Baker, D. M., and K. Davies, J. Atmos. Terr. Phys., 31, 1345 (1969).

(25) Davies, K., and J. E. Jones, J. Atmos. Sci., 28, 254 (1971).

(26) Bauer, E., et al., IDA Paper P-756 "Fluid Motions and Some of Their Effects on Chemistry of the Upper Atmosphere", (1971).

(27) Tchen, C. M., IDA Paper P-595 "Turbulence and Gravity Waves in the Upper Atmosphere", (1970).

(28) Hines, C. O., J. Atmos. Sci., 25, 937 (1968).

(29) Eckart, C., Hydrodynamics of Oceans and Atmospheres, Pergamon Press, N. Y. (1960).

(30) Shere, K. D., and I. J. Eberstein, Bull. Amer. Meteor. Soc., 51, 387 (1970).

(31) Blumen, W., and R. G. Hendl, J. Atmos. Sci., 26, 210 (1969).

(32) Chimonas, G., and C. O. Hines, Planet. Space Sci., 18, 565 (1970).

(33) Testud, J., and G. Vasseur, Gravity Waves Generated During Magnetic Substorms, presented at the International Symposium on Waves in the Upper Atmosphere, Toronto, Jan. 19-21 (1970).

(34) Murphy, E. A., et al., Trans. Amer. Geophys. Union, 52, 292, Abstract SA17, "A Statistical Distribution of Wind Shear and A Turbulence Criterion from 30 to 90 km", (1971).

(35) Justus, C. G., J. Atmos. Sci., 26, 1137 (1969).

(36) Spizzichino, A., Ann. Geophys., 25, 693 (1969).

(37) Hodges, R. R., Jr., J. Geophys. Res., 75, 4842 (1970).

(38) Bauer, E., and W. N. Podney, Bull. Am. Meteor. Soc., 51, 386 (1970).

(39) Liu, C. H., and K. C. Yeh, J. Geophys. Res., 74, 2248 (1969).

(40) Gille, J. C., J. Atmos. Sci., 25, 808 (1968).

(41) Gille, J. C., Winds and Turbulence in the Stratosphere, Mesosphere, and Ionosphere (K. Rawer Ed.), 322 (1968).

(42) Lindzen, R. S., J. Atmos. Terr. Phys., 31, 449 (1969).

(43) Woodrum, A., and C. G. Justus, J. Geophys. Res., 73, 7535 (1968).

- (44) Justus, C. G., J. Geophys. Res., 75, 2171 (1970).
- (45) Elford, W. G., and R. G. Roper, Space Research, 8, 42 (1967).
- (46) Lumley, J. L., and H. A. Panofsky, The Structure of Atmospheric Turbulence, John Wiley & Sons, New York (1964).
- (47) Lin, C. C., Statistical Theories of Turbulence, Princeton Univ. Press, New Jersey (1961).
- (48) World Data Center A: Meteorology, National Weather Records Center, High Altitude Meteorological Data (formerly Meteorological Rocket Network Firings). vol. I #1 (1966) through vol. VI #12 (1971).
- (49) Smith, W. S., et al., Temperature, Pressure, Density, and Wind Measurements in the Stratosphere and Mesosphere, NASA TR-R-211 (1964), TR-R-245 (1966), TR-R-263 (1967), TR-R-288 (1968), TR-R-316 (1969), TR-R-340 (1970), TR-R-360 (1971).
- (50) Justus, C. G., and H. D. Edwards, Tables of Observed Winds in the 70 - 170 km Region of the Upper Atmosphere, Georgia Tech, July (1965); also Montgomery, J. B., et al., AFCRL-68-0503 (1968); Justus, C. G., and H. D. Edwards, AFCRL-71-0311 (1971).
- (51) Edwards, H. D., et al., Upper Atmosphere Winds from Gun Launched Vertical Probes, U. S. Army Ballistic Research Laboratories, BRL Contract 169, Reports 1 - 10.
- (52) Bedinger, J. F., Compendium of Wind Data from the Vapor Trail Technique, GCA Technical Report No. 66-7-N (1966).
- (53) Lenhard, R. W., and A. J. Kantor, A. Catalogue of ARCAS - ROBIN Soundings, AFCRL-65-449 (1965).
- (54) Minzner, R. A., et al., Tabulations of Atmospheric Density, Temperature, and Pressure from 437 Rocket and Optical-Probe Soundings during the Period 1947 to Early 1965, GCA-TR-67-10-N (1967).
- (55) King-Hele, D. G., and D. M. C. Walker, Planet Space Sci., 17, 985 (1969) and 17, 1539 (1969).
- (56) Greenhow, J. S., and E. L. Neufeld, Proc. Phys. Soc. London, 75, 228 (1960).
- (57) Muller, H. G., Planet Space Sci., 14, 1253 (1966).
- (58) Zadorina, F. K., et al., Izvestiya, Atmospheric and Ocean Physics, 3, 3 (1967).
- (59) Spizzichino, A., Private communication of Garchy meteor wind data, see also reference (17).
- (60) Barnes, A. A., Private communication of Durham, N. H. meteor wind data.

(61) Champion, K. S. W., and A. C. Faire, Falling Sphere Measurements of Atmospheric Density, Temperature, and Pressure up to 115 km, AFCRL-64-554 (1964).

(62) Keeping, E. S., Introduction to Statistical Inference, Van Nostrand (1962).

(63) Groves, G. V., J. Atmos. Terres. Phys., 16, 344 (1959).

(64) Pokrovskiy, G. B., et al., Izv. Atmos. and Ocean Phys., 5, 631 (1969).

(65) Hines, C. O., J. Geophys. Res., 70, 17 (1965).

(66) Dutton, J. A., and G. H. Fichtl, J. Atmos. Sci., 26, 241 (1969).

(67) Miller, E. B., Atmospheric Density Variations Related to Internal Gravity Waves, NASA-CR-61359 (1971).

(68) Hyson, P., J. Appl. Meteorol., 7, 908 (1968).

(69) Miller, A. J., and F. J. Schmidlin, J. Appl. Meteorol., 10, 320 (1971).

(70) Cole, A. E., Extreme Temperature, Pressure, and Density between 30 and 80 km , Proc. 4th National Conf. on Aerospace Meteorology, Las Vegas, May (1970).

(71) Hines, C. O., J. Geophys. Res., 72, 1877 (1967).

(72) Theon, J. S., et al., Observations of Mesospheric Thermal Structure, Univ. of Illinois Aeronomy Rept. 32, Third Aeronomy Conference on Meteorological and Chemical Factors in D-Region Aeronomy, Urbana, Illinois, April (1969).

(73) MacLeod, M. A., Space Research, 9, 363 (1969).

(74) Rees, D., J. Brit. Interplan. Soc., 22, 275 (1969).

(75) Justus, C. G., J. Geophys. Res., 72, 1933 (1967).

(76) Webb, W. L., Scale of Stratospheric Detail Structure, ERDA-130, (N64 - 20309) (1964).

(77) Justus, C. G., and J. B. Montgomery, III, A Pilot Study of Irregular Winds at Chemical Release Altitudes, AFWL-TR-68-132 (1969).

(78) Peterson, J. W., and K. D. McWatters, The Measurement of Upper Air Density and Temperature by Two Radar Tracked Falling Spheres, NASA-CR-29

(79) Peterson, J. W. et al., Atmospheric Measurements over Kwajalein Using Falling Spheres, NASA-CR-218.

(80) Mahoney, J. R., and G. J. Boer, Jr., Horizontal and Vertical Scales of Winds in the 30 to 60 km Region, 3rd National Conf. on Aerospace Meteorology, New Orleans, May (1968).

(81) Cole, A. E., and A. J. Kantor, Spatial Variations in Stratospheric and Mesospheric Wind Fields, Proc. 3rd National Conf. on Aerospace Meteorology, New Orleans, May (1968).

(82) Lettau, B., Persistence of Small-Scale Features in the Mesospheric Wind Field, AFCRL-66-371 (1966).

(83) Blamont, J. E., Planet Space Sci., 10, 89 (1963).

(84) Kraichnan, R. H., Phys. Fluids, 10, 1417 (1967).

(85) Beyers, N. J., et al., J. Atmos. Sci., 23, 325 (1966).

(86) Miers, B. T., J. Atmos. Sci., 22, 382 (1965).

(87) Reed, R. J., J. Atmos. Sci., 24, 315 (1967).

(88) Reed, R. J., et al., J. Atmos. Sci., 23, 247 (1966).

(89) Reed, R. J., et al., J. Atmos. Sci., 23, 416 (1966).

(90) Reed, R. J., et al., Monthly Weather Rev., 97, 456 (1969).

(91) Greenhow, J. S., and E. L. Neufeld, J. Geophys. Res., 64, 2129 (1959).

(92) Batchelor, G. K., The Theory of Homogeneous Turbulence, Cambridge Univ. Press (1960).